INSTITUTO POLITÉCNICO DE BRAGANÇA
Escola Superior de Tecnologia e de Gestão

UNIVERSIDADE TECNOLÓGICA FEDERAL DO PARANÁ

Coupled Electromagnetic and Thermal Analysis of Electric Machines

Gabriel Dias Mendes

Supervised by:

Prof. Dr. Ângela Paula Barbosa de Silva Ferreira

Prof. Dr. Ednei Luiz Miotto

Bragança

2019 - 2020

INSTITUTO POLITÉCNICO DE BRAGANÇA Escola Superior de Tecnologia e de Gestão

UTFPR UNIVERSIDADE TECNOLÓGICA FEDERAL DO PARANÁ

Coupled Electromagnetic and Thermal Analysis of Electric Machines

Gabriel Dias Mendes

Dissertation presented to the School of Technology and Management of Polytechnic Institute of Bragança to the Fulfillment of the Requirements for the Master of Science Degree in Industrial Engineering (Electrical Engineering branch), in the scope of Double Degree with Federal University of Technology - Paraná

Supervised by:

Prof. Dr. Ângela Paula Barbosa de Silva Ferreira

Prof. Dr. Ednei Luiz Miotto

Bragança

2019 - 2020

Abstract

The actual trend of the design process of electric machines is oriented to specific requirements of the application and is no longer based in a standard structure. From this point of view, the design procedure of electric machines became a multidisciplinary process, involving electromagnetic, thermal, and mechanical modelling in a highly iterative process between the different physics fields.

This dissertation deals with the design process of electric machines, proposing a coupling methodology for the electromagnetic and thermal models which are interrelated. The electromagnetic model establishes the main losses in electric machines: iron and resistive losses. These losses are, in turn, the main heat sources, responsible for heating and temperature distribution, i.e., the object of the thermal analysis, which affects recursively the losses, due to parameter' dependency on temperature. Also, the machine temperature is crucial to maintain the lifetime of the machine. So, the coupled analysis is mandatory to achieve the nowadays requirements of higher energy efficiency and power density and cost reduction. Also, the coupled analysis enables optimization without the need to build several prototypes, making this process more time and cost-efficiency. Despite the temperature importance in electric machines, the thermal model was overlooked over the years. However, it has been receiving more attention in the past years.

In this work, the thermal modelling process is handled analytically and numerically through finite element analysis (FEA), which is also used to obtain the electromagnetic model. The modelling processes detailed during this work are applied into a study case of a single-phase transformer with the rated power of 1 kW. The numerical models were developed in the Ansys software suite, being the electromagnetic model developed in Ansys Maxwell while the thermal model has developed in Ansys Mechanical. At last, the coupling between the electromagnetic and thermal models was accomplished in Ansys Workbench.

The results obtained from the models are compared and validated with the experimental measurements of the losses and temperatures.

Keywords: Finite Element Analysis, Thermal Model, Electromagnetic Model, Coupled Analysis, Electric Machine.

Resumo

A tendência atual do processo de projeto de máquinas elétricas é orientada para requisitos específicos de sua aplicação e não é mais baseada em uma estrutura padrão. Deste ponto de vista, o procedimento de projeto de máquinas elétricas tornou-se um processo multidisciplinar, envolvendo modelagem eletromagnética, térmica e mecânica em um processo altamente iterativo entre os diferentes campos da física.

Esta dissertação trata do processo de projeto de máquinas elétricas, propondo uma metodologia de acoplamento dos modelos eletromagnético e térmico que se inter-relacionam. O modelo eletromagnético estabelece as principais perdas em máquinas elétricas: perdas de ferro e resistivas. Essas perdas são, por sua vez, as principais fontes de calor, responsáveis pelo aquecimento e distribuição de temperatura, ou seja, o objeto da análise térmica, que afeta recursivamente as perdas, pois os parâmetros são dependentes da temperatura. Além disso, a temperatura da máquina é crucial para manter a vida útil da máquina. Assim, a análise acoplada é obrigatória para atender aos requisitos atuais de maior eficiência energética e densidade de potência e redução de custos.Além disso, a análise acoplada possibilita a otimização sem a necessidade de construção de vários protótipos, tornando este processo mais eficiente em termos de tempo e custos. Apesar da importância da temperatura nas máquinas elétricas, o modelo térmico foi negligenciado ao longo dos anos. No entanto, tem recebido mais atenção nos últimos anos.

Neste trabalho, o processo de modelagem térmica é tratado analiticamente e numericamente por meio da análise de elementos finitos (FEA), que também é utilizada para obter o modelo eletromagnético. Os processos de modelagem detalhados durante este trabalho são aplicados em um estudo de caso de um transformador monofásico com potência nominal de 1 kW. Os modelos numéricos foram desenvolvidos no pacote de software Ansys, sendo o modelo eletromagnético desenvolvido no Ansys Maxwell enquanto o modelo térmico foi desenvolvido no Ansys Mechanical. Por fim, o acoplamento entre os modelos eletromagnético e térmico foi realizado no Ansys Workbench.

Os resultados obtidos com os modelos são comparados e validados com as medições experimentais das perdas e temperaturas.

Palavras-chave: Análise por Elementos Finitos, Modelo Térmico, Modelo Eletromagnético, Análise Acoplada, Máquinas Elétricas

Acknowledgments

Firstly I want to thank God for the gift of life and salvation, enabling me to accomplish this stage of my life. Without his grace and mercy, this work would not be done.

Secondly, my endless gratitude for my parents, Lourival and Lourdes, and my brother, Lucas, that helped in all stages of my life, and also believed in my potential.

This work is the result of the partnership of the Federal University of Technology - Paraná (UTFPR) and the Polytechnic Institute of Bragança, therefore I'm thankful to be part of two amazing institutions, that promoted my scientific development.

I want to acknowledge my supervisors PhD. Ângela Ferreira and PhD Ednei Miotto for their support, mentoring, patience, comprehension and honest feedback. Without their guidance, this work would not be accomplished.

Last but not least, I want to thank all my friends that supported me during this stage of my life. In especial, my double degree colleagues, Victor, João, and Henrique, who helped me during the period at Bragança.

Table of Contents

List of Figures

List of Tables

List of Abbreviations

2D	Two-dimenions
3D	Three-dimensions
AC	Alternating Current
CFD	Computation Fluid Dynamics
DC	Direct Current
FEA	Finite Element Analysis
FEM	Finite Element Method
LPTN	Lumped Parameters Thermal Network
PMM	Permanent Magnet Machine
PMSM	Permanent MagnetSynchronous Motor
TRN	Thermal Resistance Network

List of Symbols

ΔT Temperature delta, °C or K

∇T Temperature gradient, °C/m or K/m

A Surface area, m^2

B Magnetic flux density, T

C_0 Bertotti hysteresis loss coefficient

C_1 Bertotti eddy current loss coefficient

C_2 Bertotti excess eddy current loss coefficient

C_m Empirical parameter of Steinmetz's equation

D Conductor diameter, m

F Frequency, Hz

h Convection heat transfer coefficient, $W/m^2/°C$ or $W/m^2/K$

H Magnetic field strength, A/m

h_{rad} Radiation heat transfer coefficient, $W/m^2/°C$ or $W/m^2/K$

I Current, A

k Thermal conductivity, W/m/°C or W/m/K

k_R Skin effect factor

L Length, m

n_l Winding conductor layers

$P_{Bertotti}$ Bertortti iron loss, W

P_R Resistive loss, W

$P_{Steinmetz}$ Steinmetz iron loss, W

q Heat transfer rate, W

q'' Heat flux, W/m^2

R DC resistance, Ω

R_0 DC resistance at temperature T_0, Ω

R_{AC} AC resistance, Ω

R_c Transformer's core conduction thermal resistance, °C/W or K/W

R_{ch} Transformer's core convection thermal resistance, °C/W or K/W

R_{cond} Conduction thermal resistance, °C/W or K/W

R_{conv} Convection thermal resistance, °C/W or K/W

R_{cr} Transformer's core radiation thermal resistance, °C/W or K/W

R_{rad} Radiation thermal resistance, °C/W or K/W

R_w Transformer's winding conduction thermal resistance, °C/W or K/W

R_{wh} Transformer's winding convection thermal resistance, °C/W or K/W

R_{wr} Transformer's winding radiation thermal resistance, °C/W or K/W

T Temperature, °C or K

T_∞ Fluid temperature, °C or K

T_s Surface temperature, °C or K

T_{sur} Surrounding temperature, °C or K

V Voltage, V

α Resistivity temperature coefficient, $^\circ C^{-1}$ or K^{-1}

β Steinmetz's equation parameter

γ Steinmetz's equation parameter

δ Skin depth, m

ε Emissivity

λ Reciprocal of the temperature coefficient of resistance at 0 °C of the conductor material

σ Electric conductivity, S/m

σ_{SB} Stefan-Boltzmann constant, $W/m^2/K^4$

Chapter 1

Introduction

1 Introduction

1.1 Motivations

Electric machines are devices that are present in our daily activities, for instance, refrigerators, washing machines, air conditioning systems, and also in industrial and transportation applications. The aim to reduce the pollution caused by fossil fuel increased the demand for more efficient devices and energy conversion systems. According to the International Energy Agency [1], in 2018, the industry was the sector responsible for consuming 41.95% of the world electricity. So, it is clear that there is a global demand for electric machines to satisfy new applications requirements, namely power density and energy efficiency, requiring a design methodology to support this demand [2].

Electric machines are designed to fulfil the application's requirements, e.g. torque, power, speed, size. The classic design procedure is based on analytical methods to achieve the electromagnetic requirements, while the other physics domains are handled with empirical knowledge or even neglected [3]. As a consequence of the constraints and requirements of the modern application, the design procedure became a multidisciplinary process involving the relationship between different physics fields, e.g. electromagnetic, thermodynamics, acoustics, structural mechanics. Thus, this work is motivated by the necessity of handling the multiphysics nature of the electric machines in order to fulfil the requirements of modern applications.

This work is focused on the thermal modelling of electric machines and its coupling to the electromagnetic model. The thermal modelling of electric machines is crucial since the device temperature is related to its performance and lifetime. For instance, if the machine uses permanent magnets in its excitation system, for an operating temperature of 100 °C, the magnetic flux may be reduced till 20% when compared with the magnetic flux at room temperature [2], which impacts directly on the machine performance. Besides that, the temperature rise increases the resistive loss of the machine reducing the device efficiency. Additionally, there is the risk of demagnetization of permanent magnets due to the temperature rise, and if a machine surpasses its insulation limit temperature by 10 °C the insulation lifetime is cut by half [4]. Despite this strong relationship the thermal modelling of electric machines has been neglected over the years especially for small and medium-sized machines [5] but has received more attention in the past years,

in reference [6] it is possible to see the past years development to achieve better cooling solutions of power traction machines.

1.2 Electric Machines Design and Modelling

There are two types of tools used to carry out the modelling of an electric machine: analytical and numerical. Usually, the basic design and early dimensioning of the magnetic and electric circuit are done by analytical equations, and numerical methods are used to evaluate the device performance accurately [4]. Thus, both methods are used jointly to exploit their advantages and mitigate their weakness. The use of numerical methods became more popular with the advances on the digital computers, allowing an elevated amount of complex and accurate calculations in a short period. Due to nowadays computational resources, the numerical methods evolved, being able to simulate complex physics phenomena with higher accuracy, although having the trade-off to be more time-consuming along with requiring top tier computational power.

Due to the necessity to assimilate the multiphysics characteristic of electric machines coupled analysis between two or more physics fields have been developed, making the design process a high iterative process between the different physics analysis, which allows better modelling and optimization of the device, without the drawbacks of building different prototypes. Numerical methods are extensively used in coupled models since multiphysics analysis is especially problematic from the analytical point of view. Finite element analysis (FEA) is a popular numerical method that it is applicable to a variety of physical phenomena, so it is highly used in multiphysics analysis. In [7], FEA is used in the design process of a permanent magnet machine (PMM) covering the electromagnetic, stress and thermal analysis of the device. Similarly, [8] focus on the mechanical and thermal constraints to improve the rotor design of a PMM. Reference [9] uses the acoustics and structural FEA coupling to reduce the noise of a switched reluctance motor. Furthermore, in [10] the coupling analysis of electromagnetic, mechanics and acoustic is used to investigate the faults on the pressure relief system in the transformer's tank caused by external short-circuit.

The scope of this work is the electromagnetic and thermal models of electric machines. To accomplish the electromagnetic model analytically the reluctance network may be used, which is a method tipically used due to its simplicity, fast solution and reasonable accuracy, that can also be applied to model complex magnet circuits [11]–[13].

Moreover, the numerical electromagnetic modelling is mostly conducted by FEA [4] which has been used to explore design optimizations, estimate the losses in ferromagnetic materials considering the non-uniform magnetic flux density distribution, and simulating different working conditions [3], [14]–[17].

Concerning the thermal model, it can be achieved analytically through thermal resistance network (TRN), which is also known as lumped parameters thermal network (LPTN), and numerically by using FEA or computational fluid dynamics (CFD) [18]. TRN is widely used [19]–[21] due to its simplicity along with a reasonable error since it is basically analysed trough a dual electric circuit, allowing to use tools such as circuit simulators to obtain the temperature results of the model. Therefore the method's challenge is to calculate the thermal resistances correctly, putting significant effort to model the main heat paths [18]. However, the modelling of the thermal resistances of complex parts can be very difficult and complicated to predict hot spots with enough accuracy [22].

FEA is commonly used in thermal models [23]–[25] since it allows a massive discretization of the geometry resulting in the precise temperature distribution of the device, depending essentially on the accuracy of the thermal parameters used in the model. The drawback of the FEA is that it relies on empirical relations to obtain the convections coefficients, that it is also present in the TRN approach, so when the cooling system of the machine involves complex fluid flow systems, the CFD takes place, being used to simulate the fluid flow of the system and calculate its convection coefficient, which was successfully used in [26]–[28]. Nonetheless, the CFD has the drawback of being demanding on massive time and computational resources. Therefore hybrid approaches combining CFD with FEA and TRN are usually used, like the one proposed in [22] to model railway traction motors.

1.3 Objectives

Within the context set by the previous sections, the objectives of this work are summarized in:

- Establish the main aspects of the heat generation and transfer on electric machines that are necessary to understand the thermal model and its characteristics, highlighting the relationship between the thermal and electromagnetic analysis.

- Discuss the main analytical and numerical methods to achieve the thermal model of electric machines, guiding through each modelling step.
- Develop a coupled electromagnetic and thermal analysis, to aid in the design and derating process of electric machines.
- Apply the modelling methods discussed in this work in a study case, for comparison and validation purposes.

1.4 Structure of the Work

Besides this chaper that presents the introduction of the work, covering the motivations, objectives, and the state-of-the-art of the electric machines modelling process, the dissertation' form is structured as follows:

- Chapter 2: addresses the existing heat sources in electric machines and the heat transfer mechanisms as well.
- Chapter 3: discusses analytical thermal modelling is and presents the development process of three-dimensional TRN.
- Chapter 4: presents the electromagnetic and thermal numerical modelling through FEA, and proposes the coupling methodology between the two analyses.
- Chapter 5: the results obtained from the models developed for the work's study case are compared and confronted with experimental measures.
- Chapter 6: presents the main conclusions of the work, also draws the aims for the future works related to this project.

Chapter 2

Heat Generation and Transfer

2 Heat Generation and Transfer

The power losses in electric machines are typically low when compared with the rated power, although, they are capable of heating their components to temperatures where the performance and lifetime are affected. Therefore, the device heat management is necessary to grant its proper working conditions. This chapter addresses the principal heat sources in electric machines and establishes the heat transfer background.

2.1 Heat Generation

Heat generation in electric machines occurs due to the losses present in the machine. These losses can be separated into three categories, mechanical loss, electromagnetic loss, and additional losses. Mechanical loss is present in rotating machines and relates with ventilation and bearings friction. Electromagnetic losses are the losses originated by the Joule heating in the windings, i.e., resistive loss, and the loss in the magnetic circuit, iron loss. The additional losses consist of the electromagnetic loss not included by the resistive and iron losses. They are related to the non-uniform distribution of the current in the windings and to iron loss produced by the distortion of the magnetic flux caused by the load current, and the iron loss that occurs in the machine frame [29]. These losses are not determined by mathematical models since they are difficult to model and calculate. Thus IEC standards define the additional losses as a portion of the input power [4].

The purpose of this section is to discuss and model the resistive and iron losses since they correspond to the majority of the power loss in electric machines.

2.1.1 Resistive Loss

Resistive loss is the main loss source of an electric machine, they occur due to the damping forces into the conductor, causing collisions between the atoms of the conductor and the electric charges from the electric current flowing through the conductor, dissipating energy in the heat form. This phenomenon is expressed by Joule's first law

$$P_r = I^2 R \tag{2.1}$$

where I is the rms value of the current flowing through the conductor, and R is the direct current (DC) resistance of the conductor.

Conductors under alternating current (AC) excitation can suffer from the skin effect phenomenon, which increases the resistance and consequently the resistive loss. This phenomenon occur due to the limitation of how much an electromagnetic wave can

penetrate in a conductor, limiting the current flow surface area. The skin depth, δ, determines how much the wave can penetrate the conductor and it is given by

$$\delta = \frac{1}{\sqrt{\pi f \mu \sigma}} \tag{2.2}$$

being f the frequency of the current, μ the permeability and σ the conductivity of the conductor. As δ is frequency dependent, it is necessary to evaluate in the frequency range of the machine and for the significant harmonic components of the current. Table 2.1 shows the frequency influence on skin depth of the copper with $\sigma = 5.8 \times 10^7$ S/m, and permeability equal to the free space. It is possible to see the impact of this phenomenon at high frequencies.

Table 2.1 Skin depth in copper. Adapted from [30]

Frequency (Hz)	**10**	**50**	**100**	**500**	**10^4**	**10^8**	**10^{10}**
Skin depth (mm)	20.8	8.6	6.6	2.99	0.66	6.6×10^{-3}	6.6×10^{-4}

Considering the skin effect, the resistive loss is given by

$$P_r = I^2 R_{AC} = I^2 k_R R \tag{2.3}$$

where R_{AC} is the AC resistance of the conductor, which is obtained by multiplying the DC resistance by the skin effect factor k_R [4], being dependent of the geometry and material of the winding. For a round wire it can be approximated by

$$k_R \approx 1 + 0.59 \frac{n_l^2 - 0.2}{9} \frac{D^4}{\delta^4} \tag{2.4}$$

being n_l the number of conductors layers, and D the diameter of the conductor. For frequencies of the fundamental component and significant harmonic components where δ is equal or higher than the conductor width, the skin effect factor, k_R, can be considered equal to 1.

The resistive loss has a strong relationship with the temperature, as the temperature increases the resistance also increases. This dependence is expressed by

$$R(T) = R_0 \left[1 + \alpha (T - T_0)\right] \tag{2.5}$$

where R_0 is the value of the resistance at the temperature T_0, α is the temperature coefficient of resistivity, that for materials typically used in windings such as the copper and aluminium is respectively $3.81 \times 10^{-3}\ °C^{-1}$ and $3.7 \times 10^{-3}\ °C^{-1}$ [4], and T is the actual temperature of the conductor. Using equation (2.5) it is possible to see that a

temperature rise of 55 °C in a copper wire, will result in a 20.96% increase of the resistance, thus increasing the resistive loss.

2.1.2 Iron Loss

Iron loss is related to the phenomenon of magnetization in the ferromagnetic materials used to create the magnetic flux path. It occurs due to the eddy currents flow on the ferromagnetic material, causing Joule heating [31], and by the hysteresis loss caused by the rotation of the magnetic dipoles on the ferromagnetic material, causing friction between the neighbouring domains, thus energy consumption [32]. Despite the origin of the iron loss being well-known, mathematical modelling still a challenge nowadays. This is because of the complexity of the phenomena involved, requiring simplifications and assumptions, the physical phenomena occur at a microscopic level, and the loss formulation are developed at a macroscopic level.

In practice, the iron loss estimation is accomplished by empirical models or equations based on the physical phenomena [33]. The usual approach to model iron loss is to separate it into two distinct components, hysteresis and eddy current losses. The eddy current loss is calculated for a uniform magnetization, which does not occur in practice, and as consequence the eddy current loss is much higher than the calculated. Thus, to compensate this error, iron loss model considers a third portion to the iron loss, known as excess eddy current loss or anomalous loss [34]. An example of the loss separation method is the Bertotti model for sinusoidal magnetization [35],

$$P_{Bertotti} = C_0 B_{\max}^2 f + C_1 \left(B_{\max} f\right)^2 + C_2 \left(B_{\max} f\right)^{1.5} \tag{2.6}$$

where $B_{\max}$ is the maximum value of the magnetic flux density, C_0 and C_2 are the coefficients related to the hysteresis and excess eddy current losses, being obtained from experimental measures, C_1 is the eddy current loss coefficient that is obtained by

$$C_1 = \frac{\pi^2 \sigma d^2}{6} \tag{2.7}$$

being σ the electric conductivity and d the thickness of the electrical steel sheet. From the equation above, it is possible to see the relation between the eddy current loss and the thickness of the iron sheet, enlighten the reason why eddy current loss is massive on solid objects.

Bertotti model has the drawback of being suitable only for applications under sinusoidal magnetization at a limited frequency range, which is not the case for most

electric machines. To cover this drawback, models considering the effect of typical non-sinusoidal waveforms were developed, for instance [36], where the average and rms characteristics of the supply voltage are used to consider different waveforms, obtaining errors of 5% to 6% of the loss prediction on the transformers used, and for induction motors the errors were between 10%-20% In [37] are used the peak voltage and duty cycle of the waveform, which resulted in a very good agreement with the experimental data available for low and high frequency applications.

Many material sciences specialist contradicted the loss separation approach [38]. Graham in [31] establishes that there is no physical distinction between the hysteresis loss and eddy current loss, the iron loss occurs whenever the magnetization changes, which is done by domain wall motion, generating eddy currents and consequently loss. The Steinmetz model is a well-known empirical equation that does not separate the iron loss into different components,

$$P_{Steinmetz} = C_m f^{\gamma} B_{\max}^{\beta} \tag{2.8}$$

where C_m, γ and β are empirical parameters obtained by fitting experimental curves [39], and f is the frequency of the magnetization. Since this model was developed more than a century ago, it is applicable only for sinusoidal magnetization. To apply this model in applications with non-sinusoidal magnetization, researchers developed modified versions to obtain an accurate prediction for arbitrary waveform, as the ones proposed in [38] and [39], where it is used an equivalent frequency to model the waveform impact on the iron loss.

One of the difficulties of calculating the iron loss is the fact that magnetization is not uniformly distributed and, consequently, neither the losses are. This characteristic sheds light to the FEA approach [14], [15], [17], since the FEA computes the flux density for all elements of the geometry, enabling to calculate the loss for each element, therefore getting the loss distribution on the geometry.

The iron loss is strongly dependent on the material properties, their characteristics can vary about 30 % between different batches, and even in the same batch [40], bringing a level of uncertainty between the specification sheet of the manufacturer and the actual material used to build the electric machine. Mechanical stress caused by the manufacturing process of shrink fitting and operating conditions of the machine also affects the iron losses, studies were developed aiming the prediction and mitigation of this factor [41]–[43].

Differently from the resistive loss, the iron loss decreases with the temperature increase. As the resistivity of the material increases with the temperature rise the eddy currents are reduced, and consequently the heat dissipation. Several models considering the temperature influence in iron loss have been developed. For instance, in [39] the temperature influence is added to the Steinmetz model and in [16], [44], [45] the temperature dependency is included to the separation loss model. The experimental data of the iron loss in [16] reported that for a variety of frequencies and current loads the temperature rise from 69°C to 100°C resulted in a maximum reduction of 12% of the iron loss. Although, the temperature can have more impact on the iron loss for situations where the machine operates at high temperature levels. Thus, the loss prediction without the temperature dependency will result in a slight overestimation of the loss value.

2.2 Heat Transfer

Heat transfer is energy in transit due to a temperature difference, meaning that heat transfer must occur whenever there is a temperature difference[46]. This temperature difference can be between different physics states of matter, as a kettle (solid) and the water (liquid), and even without a material medium between them (ultraviolet radiation). The heat transfer occurs by three different modes: conduction, convection, and radiation.

2.2.1 Conduction

Heat transfer by conduction is related to the interaction between particles of a substance. The particles with more energy, that also have higher temperatures, will transfer energy to the surrounding particles with less energy. By this way, the heat flow by conduction will occur from the higher temperature parts to the lower temperature spots. Conduction occurs in the three states of matter, but within the electric machine context the conduction is restrained to the solid-state, where the energy transport occurs by free electrons and lattice vibrations[47].

The heat transfer rate is given by the Fourier's law of heat conduction

$$q_{cond} = - kA \nabla T \tag{2.9}$$

expressing that the heat flow q is given by three parameters: thermal conductivity k of the material, area A normal to the heat flow, and temperature gradient ∇T of the geometry. The thermal conductivity parameter shows how much the material allows the heat flow. The heat flux can be obtained from the equation (2.9):

$$\frac{q_{cond}}{A} = q''_{cond} = -k\nabla T \tag{2.10}$$

The minus sign means that the heat is transferred from the higher temperature to the lower temperature. Using a 3D cartesian coordinated system (x, y, z) and considering an isotropic material, whereas k is constant for all directions, the heat flux assumes the following form:

$$q''_{cond} = -k\left(\hat{\mathbf{i}}\frac{\partial T}{\partial x} + \hat{\mathbf{j}}\frac{\partial T}{\partial y} + \hat{\mathbf{k}}\frac{\partial T}{\partial z}\right) \tag{2.11}$$

For anisotropic materials that have different thermal conductivities for each direction, equation (2.11) can be written as

$$q''_{cond} = -\left(\hat{\mathbf{i}}k_x\frac{\partial T}{\partial x} + \hat{\mathbf{j}}k_y\frac{\partial T}{\partial y} + \hat{\mathbf{k}}k_z\frac{\partial T}{\partial z}\right) \tag{2.12}$$

Not all cases need to be treated as a 3D heat conduction problem, it is possible to assume that there will not have heat transfer in a specific direction, due to negligible temperature difference or due to the lower thermal conductivity value when compared to the others directions.

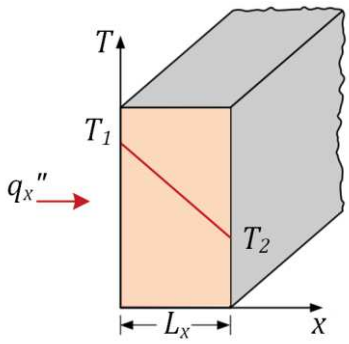

Figure 2.1 One-dimensional heat transfer by conduction (Adapted from [46]*)*

The heat flux in the x-direction, illustrated in Figure 2.1, under steady-state condition is

$$q''_x = -k_x\frac{T_2 - T_1}{L_x} \tag{2.13}$$

where L_x is the path length that separates the temperatures T_1 and T_2. This steady-state equation applies to the other directions as well.

Since the conduction is dependent on the material medium, it is necessary to determine the thermal conductivity of the material used in the devices. Generally speaking, good electric conductors are also good thermal conductors, e.g. copper thermal

conductivity is 394 W/m/°C, and electric insulators are also thermal insulators, e.g. *k* for a typical insulation system of an electric machine is 0.2 W/m/°C. It should be mentioned that the thermal conductivity is temperature dependent: thermal conductivity decreases with increasing temperature for thermal conductors and increases it for thermal insulators [4].

2.2.2 Convection

Convection is the heat transfer between a higher temperature region and a region of cooler temperature [47], that is based on the energy transfer due to diffusion and motion of the fluid. In this section will be developed to the heat convection between a surface.

In Figure 2.2, a surface (hot block) is in contact with a fluid (air), the temperature of the surface T_s is higher than the fluid temperature T_∞, so the heat of the hot block will be transferred to the fluid. First, the heat transfer will occur by conduction from the surface to the air layer adjacent to the surface, then the convection will be removing the heated air and replacing it with cooler air.

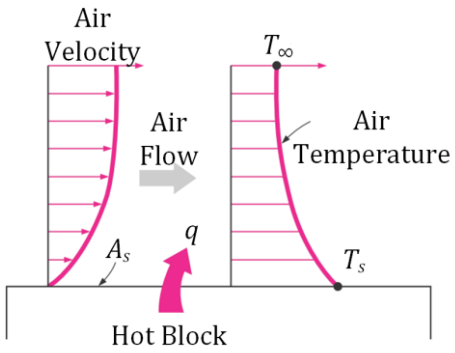

Figure 2.2 Convection between surface and air (Adapted from [47]*).*

The velocity of the air on the surface is 0 m/s, but as soon the air takes distance from the surface the velocity of the air will increase, implying a velocity gradient. Similarly, the air will have a temperature gradient, the air temperature will be higher near the surface, a value close to T_s, and it will decrease with the distancing of the surface.

There are two types of convection, natural and forced convection, being the difference between them the origin of the fluid motion. Regarding natural convection, the fluid motion is caused by buoyancy forces due to the density difference caused by temperature difference. Forced convection is based on the fluid motion induced by external forces, such as a fan and a pump. Figure 2.3 illustrates both types of convection.

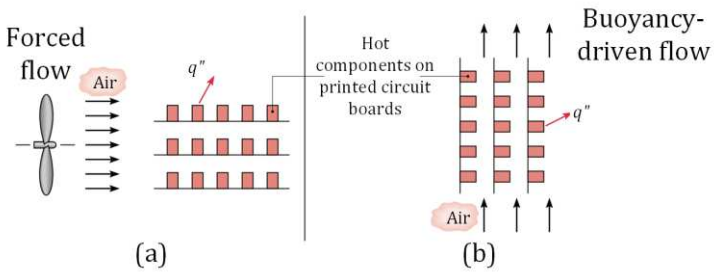

Figure 2.3 Convection heat transfer types. (a) Forced convection. (b) Natural convection. (Adapted from [46]*).*

Independently of the type of convection, the heat transfer rate by convection is given by Newton's law of cooling

$$q_{conv} = hA_s(T_s - T_\infty) \tag{2.14}$$

where h is the convection heat transfer coefficient, A_s is the surface area, T_s the surface temperature, and T_∞ the fluid temperature. This is a simple equation, but the challenge of convection is on determining h. This coefficient is dependent on many factors, such as the surface geometry and roughness, the fluid properties e.g. density, dynamic viscosity, specific heat, etc., and the type of fluid flow [47].

The convection heat transfer coefficient, h, is tipically defined through empirical relations or computational fluid dynamics simulations [48]. Table 2.1 presents the value range of h for some convection processes, highlighting the difference of the cooling performance between the forced and natural convection, and also between the gases and liquids.

Table 2.1 Typical values of the convection heat transfer [46]

Process	**h [W/ m^2/°C]**
Free Convection	
Gases	2-25
Liquid	50-1000
Forced Convection	
Gases	25-250
Liquids	100-20,000

2.2.3 Radiation

Radiation is the energy emitted by matter in the form of electromagnetic waves [47], due to changes in the electron configurations of the atoms or molecules, the wavelength of which lies in the range from 0.1 to 100 μm [4]. One of the most important properties of the radiation is that it does not require a material medium. The radiation can occur from

gases, liquids, and solids, but for electric machines, the focus is on the radiation from solids surfaces.

The thermal radiation is the radiation emitted by a surface due to its temperature, and the maximum emissive power of a surface is given by the Stefan-Boltzmann law

$$E_b = \sigma_{SB} A_s T_s^4 \tag{2.15}$$

where σ_{SB} is the Stefan-Boltzmann constant that is equal to 5.67×10^{-8} W/m^2/K^4, A_s is the surface area, and T_s is the surface temperature. This equation considers an ideal surface emitting at the maximum rate, i.e., a blackbody.

Real surfaces cannot emit at the maximum rate, so the equation (2.15) becomes

$$E = \varepsilon \sigma A_s T_s^4 \tag{2.16}$$

where ε is the emissivity of the surface that is dependent on the material, which varies from 0 to 1. It should be noted that, when ε = 1, the surface is a blackbody.

Figure 2.4 shows a typical situation, where larger surfaces surround a smaller surface, e.g. a room surrounding a motor frame. For such cases, the net rate of radiation heat transfer between the surface and its surrounding is

$$q_{rad} = \varepsilon \sigma A_s \left(T_s^4 - T_{sur}^4\right) \tag{2.17}$$

being T_{sur} the surrounding surface temperature [47].

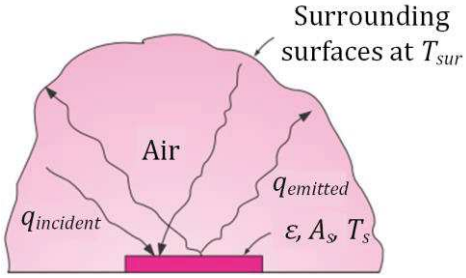

Figure 2.4 Radiation heat transfer (Adapted from [47]*).*

The emissivity of a black body surface is constant for all directions, this means that it is a diffuse emitter. For real surfaces, the emissivity is not constant for all directions as illustrated in Figure 2.5. Since the ratio between the emissivity in the normal direction and in different directions is at maximum 30% for conductors and 5% for non-conductors, it is reasonable to considerate the surface emissivity for all directions as the emissivity in the normal direction [46].

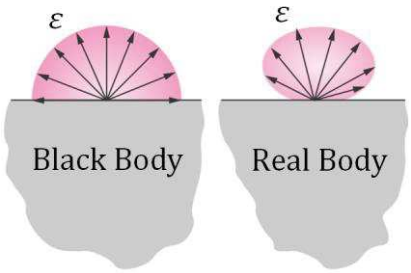

Figure 2.5 Directional distribution of emissivity (Adapted from [47]*).*

2.3 Summary

This chapter discussed the main aspects of heat generation and heat transfer regarding electric machines, detailing the physics phenomena and formulation of the main losses found in electric machines. Also, the fundamentals of heat transfer necessary to understand the thermal modelling process were briefly introduced. All three modes of heat transfer are important in the thermal management of electric machines. Still, convection is the primary mechanism to remove the heat from the device to the ambient, along with the radiation, which has the performance similar to the natural convection. Conduction is important to provide an efficient thermal flow, granting that inner heat flows to the surfaces performing convection and radiation.

Chapter 3

Analytical Thermal Modelling

3 Analytical Thermal Modelling

In this chapter will be discussed the analytical thermal modelling of electric machines by using the thermal resistance network approach. The concepts of this method are presented, and the thermal modelling of an electric machine is described. The topic under discussion is developed by applying the thermal resistance network analysis to a single-phase transformer.

3.1 Thermal Resistance Network

The thermal resistance network (TRN) is an analytical method to model and solve steady-state heat transfer problems by using the analogy between the heat flow and electric circuits. It consists of the discretization of the problem domain into thermal resistances, therefore with more discretization and more detailing the accuracy of TNR will increase, but it also increases the complexity of solving and modelling.

Electric flow or electric current is defined by the well know Ohm's law

$$I = \frac{V}{R} \tag{3.1}$$

which establishes the current I as the ratio of the potential difference V, or voltage, and the electric resistance R. Comparing the analysis of electric circuits to the heat transfer problem, it is possible to establish the followings analogies. The electric current occurs due to a potential difference applied to electric resistance, in a similar way the heat flow occurs due to a temperature difference. The electric current follows the path defined by the electric resistance, so the thermal resistance defines the path of the heat flow as well.

With this analogy, it is possible to solve a heat transfer problem by solving its dual electric circuit, where the current is replaced by the heat transfer rate q, the voltage by the temperature difference, and the electric resistance by the thermal resistance. As the thermal circuit is replaced by its dual electric circuit, the well-consolidated tools to solve electric circuits can be exploited to solve the thermal circuit.

The temperature output of a TRN can be expressed as a matrix

$$[\boldsymbol{T}] = [\boldsymbol{R}_t]\,[\boldsymbol{q}] \tag{3.2}$$

which is equal to the thermal resistances matrix multiplied by the heat transfer rate matrix. Each node presents a temperature output, therefore, if more temperature outputs are wanted, more resistances are necessary, resulting in more discretization of the

problem domain. To perform an appropriate TRN it is necessary to evaluate what level of discretization is necessary, and what domain region requires more discretization and detail level.

Heat transfer is a three-dimensional phenomenon, but for some cases, i.e., anisotropic materials, it is possible to neglect the heat transfer in one direction, facilitating the TRN modelling. Additionally, because most thermal resistances are temperature dependent, the TRN resolution requires an iterative solution process, to model accurately the process.

Section 3.3 explains the process to obtain the thermal resistance for each heat transfer mode.

3.2 Thermal Resistance Network of Electric Machines

The use of TRN in electric machines is very convenient since engineers are familiar with complex electric circuits. This method has been used for complex and modern electric motors, such as the ones at the Formula E [21]. The study presented in [20] developed a thermal network model for industrial induction motors, that resulted in a ± 5 °C error between the TRN and the measured temperatures of the tested motor. The authors of [19] also exploit the entropy generation to develop a thermal network of an induction motor used to drive an electronic submersible pump.

The work developed in [49] exploits a TRN of a vehicle claw-pole alternator, and investigates the improvement given by calibrating the convection coefficients used in the model. A TRN of a 10 MW wind turbine is modelled in [50] and the results are compared to 2D and 3D finite-element analysis, presenting temperature difference around 10%.

Despite of its simplicity the TRN is being widely used, receiving improvements according to the needs of the project. It presents the flexibility of making a simple network to obtain a quick temperature output with a certain error, or to make a detailed and precise network without the need of a high computational power. Its usage on modern applications shows that this method is relevant even with nowadays powerful computers and software.

3.2.1 Heat Generation

The losses in electrical machines were previously explained in chapter 2. These losses are incorporated in the TRN as current sources, and the way those losses are distributed in the TRN has a significant impact on the model. The losses can be modelled by a single

current source, or they can be split in the TRN in a way that is more suitable to the heat generation that occurs in the machine.

A precise heat generation distribution is not easy, since the losses are not uniformly distributed and is difficult to have the losses distribution within the geometry. However, it is recommended to put some effort in the allocation process of the heat sources, according to the available information about the losses distribution.

3.3 Thermal Resistances

The challenge is to determine the thermal resistance since the heat transfer occurs by three different modes, naturally, each mode will have a different resistance formulation.

Establishing the resistance as the ratio of the driving potential and the corresponding transfer rate [46], a generic thermal resistance will be

$$R_t = \frac{\Delta T}{q} \tag{3.3}$$

Where ΔT is the temperature difference, and q the heat transfer rate.

3.3.1 Conduction

Heat transfer by conduction is responsible for the main heat flow within the machine material medium. Its correct modelling is crucial because it models the heat transfer paths of the machine, as stated by [18], which emphasizes the importance of the effort to model accurately the heat-transfer paths.

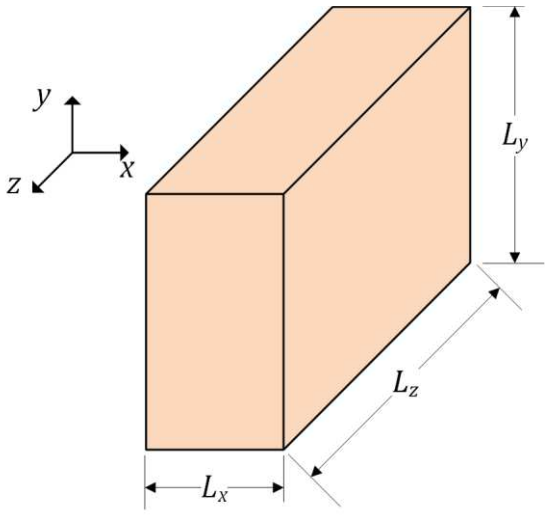

Figure 3.1 Rectangle bar

By using equation the thermal resistance for conduction, or conduction resistance, is defined as

$$R_{cond} = \frac{L}{kA} \tag{3.4}$$

where L is the length of the heat transfer path, k the thermal conductivity, and A the cross-section area. So, the thermal resistance of the Figure 3.1 bar for the the x-direction conduction is

$$R_{cond,x} = \frac{L_x}{k_x L_y L_z} \tag{3.5}$$

Having one resistance on the x-direction gives the temperature information of the two-ends of the bar, so to obtain more temperature outputs, it is necessary to divide the path length according to the desired number of outputs and the desired temperature spot. The same logic is applied to the other directions.

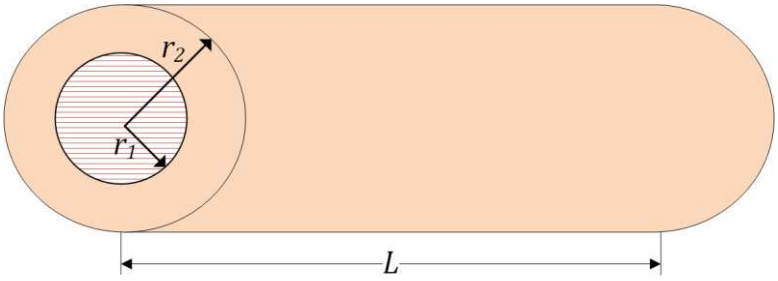

Figure 3.2 Hollow cylinder

As several electric machines have a hollow cylindrical shape, for instance their stator core, the thermal resistance for conduction in the radial direction is estimated through

$$R_{cond} = \frac{\ln(r_2/r_1)}{2\pi kL} \tag{3.6}$$

being r_2 the outer radius, r_1 the inner radius, and L is the length of the cylinder.

The conduction resistance of the winding is a complex challenge, due to its heterogeneous compound characteristic, and not uniformly geometry. As the windings are the main source of heat, and it is where the higher temperatures are spotted, several research focused on the windings conduction resistance were done, as the ones presented in [51]–[55].

3.3.2 Convection

From equation the thermal resistance for convection, or convection resistance, is obtained

$$R_{conv} = \frac{1}{hA} \tag{3.7}$$

where h is the convection heat transfer, and A is the surface area in contact with the fluid. The challenge of the convection resistance is to obtain h, since it is dependent on many factors, such as the type of fluid motion, the fluid used to cool the system.

By dividing the machine geometry into basic geometries it is possible to use the convection relations available in heat transfer references, e.g. [46], [47], [56]. The following equation $h = 1.42\left(\frac{\Delta T}{L}\right)^{0.25}$ is an example of a relation available in [47], expressing h for a vertical plane with free air convection, where ΔT is the temperature difference, in Celsius, between the surface and the air, and L is the length of the plate.

So the convection resistance of the surface in Figure 3.3 is

$$\begin{aligned} R_{conv} &= \frac{1}{hL_x L_y} \\ h &= 1.42\left(\frac{\Delta T}{L_y}\right)^{0.25} \end{aligned} \tag{3.8}$$

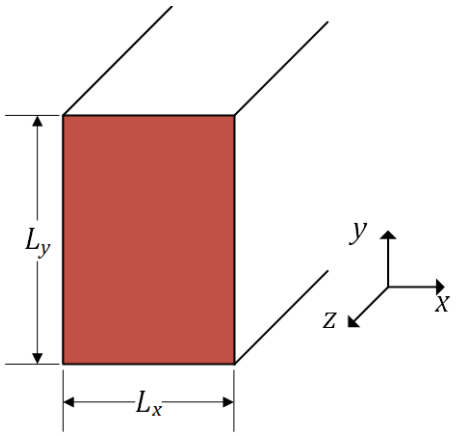

Figure 3.3 Convection surface

Although the equation is very simple, it addresses the temperature dependency of the convection coefficient, which leads to an iterative process to obtain the convection resistance, variable with the temperature results.

For machines with complex convection cooling systems, e.g. water jacket, oil spray, oil as cooling fluid, it is necessary to put more effort to obtain the coefficients since these cooling systems are more complex and the physics involved is not straightforward.

3.3.3 Radiation

Similarly to the convection resistance, the thermal resistance for radiation, or radiation resistance is

$$R_{rad} = \frac{1}{h_{rad} A} \tag{3.9}$$

where A is the surface area in contact with the surrounding and h_{rad} is the radiation heat transfer coefficient, which is given by

$$h_{rad} = \varepsilon \sigma_{SB} (T_s + T_{sur}) (T_s^2 + T_{sur}^2) \tag{3.10}$$

being ε the surface emissivity, σ_{SB} the Stefan-Boltzmann constant, T_s the surface temperature and T_{sur} the surrounding temperature.

Although the surface emissivity is not the same for all directions, it is possible to approximate the emissivity of the surface to its emissivity in the normal direction, since the difference is rarely higher than 30% [46]. To increase the radiation performance is possible to choose the paint that has high emissivity.

The heat transfer through radiation is significant in electric machines, on the inside and out of the machine. The authors of [57] evaluated the thermal resistances for radiation of an induction motor, concluding that thermal radiation outside and inside of the machine is comparable to free convection, pointing out the importance of the thermal radiation on systems without forced convection. The main radiation paths inside the machine are between the wires inside the slot and the stator lamination, and between the end winding and the external frame.

3.3.4 Volume Element

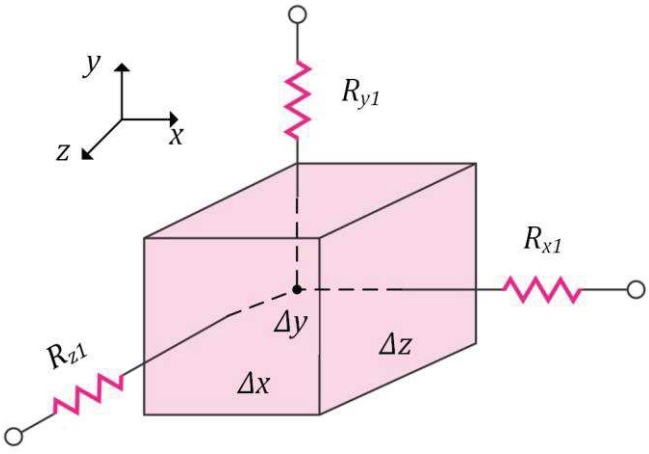

Figure 3.4 Volume element (Adapted from [56]*)*

Obtaining a TRN of a 3D geometry can be easily developed recurring to the volume element method. Figure 3.4 shows a generic volume element for a cartesian coordinate system, the subscript identifies the resistance axis.

By dividing the geometry into volume elements, the process of modelling the thermal resistances and the connections between the resistances becomes easier. Using more volume elements will lead to more precise results since the problem will have more discretization.

3.4 Analytical Thermal Modelling of a Low Power Transformer

To detail the process of modelling an electric machine, the analytical thermal modelling method presented in this chapter was applied to model a low power single-phase transformer. This transformer was chosen as case study of this work because, being the first approach of the author to model electric machines, it is a simple static electric machine, not involving mechanical loss and other aspects present in rotational machines, and due to its availability in the laboratory to perform experimental tests. Appendix A contains the details and characterization of the used transformer.

3.4.1 Transformer Geometry

The first step of thermal modelling is to spot the symmetry characteristics of the geometry. Exploiting the symmetry characteristics allows a higher level of discretization and detail, without the drawbacks of handling with so many resistances.

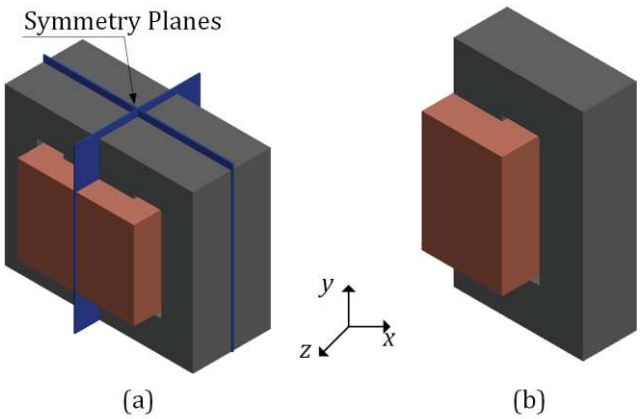

Figure 3.5 Transformer geometry: (a) Symmetry characteristic (b) Modelled geometry

Figure 3.5 shows the transformer geometry and exploits its symmetry characteristics, so it is possible to see the existence of two symmetry planes, meaning that it is only necessary to model ¼ of the transformer.

The following step consists in this geometry modelling into volume elements, such as the one proposed in Figure 3.4, and connecting the volumes according to the direction or directions that the volumes have contact. Each volume will have the number of thermal resistances according to the contact that they make with other volumes, and with the ambient.

3.4.2 Transformer Losses

The transformer is a static machine, thus the transformer losses correspond only to the resistive loss on the windings, and to the iron loss on the core. Appendix A details the procedure to obtain the losses experimentally.

It was assumed that the heat generation in the transformer occurs uniformly in each material type, i.e, core and windings, although iron and resistive losses are dependent of the iron saturation levels and current density, respectively, which are not uniform within the machine. This simplification is assumed due to the fact that a non-uniform distribution would require more detailing and inputs from the electromagnetic model. By this way, the heat generated in the core will be equally distributed to all core's volumes elements, and the same development applies to the windings. Therefore, beyond the thermal resistances, each transformer's volume element has a heat source, modelled as a current source.

Table 3.1 Transformer losses

Source	Full Loss (W)	¼ Loss (W)	Elements	Element Loss (W)
Core	13	3.25	18	0.1806
Low Voltage Winding	29.26	7.32	4	1.8290
High Voltage Winding	20.34	5.09	4	1.2713

Table 3.1 details the modelled heat distribution. As the TRN represents only a ¼ of the transformer, the losses in the TRN corresponds to ¼ of the total losses. At last, the loss value is divided by the number of elements, according to the geometry discretization underuse.

3.4.3 Transformer Volume Element Modelling

The objective of this section is to explain the process of obtaining the volume elements thermal resistances and how they are connected with the ambient, and other volumes. The same modelling process was applied to all volume elements, so for the sake of simplicity, the process of a single volume element will be detailed.

Figure 3.6 (a) shows the volume elements of the core. In order to allow a better visualization, labels of the volumes behind the ones numbered were omitted, being 9 plus the volume number in the front. For example, the volume behind V_{c1} is V_{c10}. And Figure 3.6 (b) shows the windings volume elements, the element V_{w6} and V_{w8} are below V_{w5} and V_{w7}, respectively, therefore it is not possible to visualize these two elements.

An important aspect to point out about this model is the fact that it considers there is no heat transfer between the modelled portion of the transformer and its symmetry counterpart. For example, it is not considered the heat transfer between V_{c2} and the neighbour from the other side of the symmetry plan. The model assumes a symmetry boundary condition, i.e., the temperature of V_{c2} is equal to the one of neighbour volume, which in fact translates in neglecting the conduction resistance between them. Due to the small temperature difference between the volumes near the boundary regions this simplification is admissible. The results obtained from the thermal FEA (chapter 4) corroborates with this simplification applied to the analytical model.

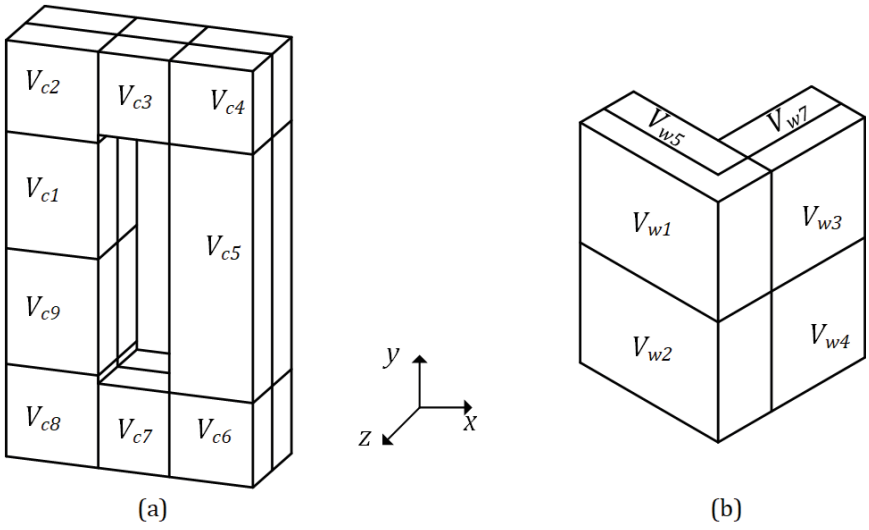

Figure 3.6 Transformer volume elements: (a) core and (b) windings.

Figure 3.7 shows the surfaces that perform convection and its corresponding convection heat transfer coefficient, for aesthetic reasons, the winding surface facing down (plane *xz*) is omitted, its corresponding coefficient is h_{w3}. As the surfaces for radiation and convection are the same, the label pattern of the radiation heat transfer coefficient follows the same numbering of the convection coefficient of Figure 3.7, only adding the subscript *r*, e.g. h_{rc1}, h_{rw2}, whereas subscripts *c* and *w* correspond to core and winding elements, respectively.

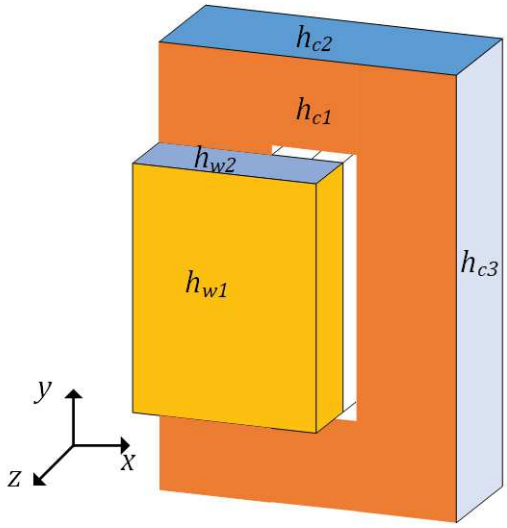

Figure 3.7 Convection coefficients

The volume element chosen to explain the process is V_{c4} because it is in contact with other volumes and air. So, it is necessary to model the thermal resistances of the volume in all three directions, and the resistances related to the convection and radiation.

First, the focus will be in the heat flow through V_{c4} occurring in the *x*-direction. The heat transfer occurs from V_{c3} to V_{c4}, and from V_{c4} to the ambient. So, one conduction resistance connects V_{c3} to the middle point of V_{c4}, and a similar resistance connects V_{c4} to the convection and radiation resistances, which are connected to the temperature ambient. Since the heat is flowing in the *x*-direction the surface plane related to the radiation and convection is the plane *yz*. For the *y* and *z*-directions this same logic is applied, resulting in the TRN displayed in Figure 3.8.

Using the generic dimensions of Figure 3.4, the conduction thermal resistances of V_{c4} are

$$R_{c4x1} = R_{c4x2} = \frac{\Delta x}{2k_{cx}\Delta y\Delta z} \tag{3.11}$$

$$R_{c4y1} = R_{c4y2} = \frac{\Delta y}{2k_{cy}\Delta x\Delta z} \tag{3.12}$$

$$R_{c4z1} = R_{c4z2} = \frac{\Delta z}{2k_{cz}\Delta x\Delta y} \tag{3.13}$$

being Δx, Δy, Δz the element dimensions for each direction, and k_c the thermal conductivity of the core in the direction specified by the correspondent subscript.

And for the convection and radiation, the thermal resistances are.

$$R_{c4hxy} = \frac{1}{h_{c1}\,\Delta x \Delta y} \tag{3.14}$$

$$R_{c4rxy} = \frac{1}{h_{rc1}\,\Delta x \Delta y} \tag{3.15}$$

$$R_{c4hxz} = \frac{1}{h_{c2}\,\Delta x \Delta z} \tag{3.16}$$

$$R_{c4rxz} = \frac{1}{h_{rc2}\,\Delta x \Delta z} \tag{3.17}$$

$$R_{c4hyz} = \frac{1}{h_{c3}\,\Delta y \Delta z} \tag{3.18}$$

$$R_{c4ryz} = \frac{1}{h_{rc4}\,\Delta y \Delta z} \tag{3.19}$$

The subscript of each resistance specifies the heat transfer mode, *r* and *h* for radiation, and convection, respectively, and the surface plane involved. The coefficients of heat transfer are according to Figure 3.7.

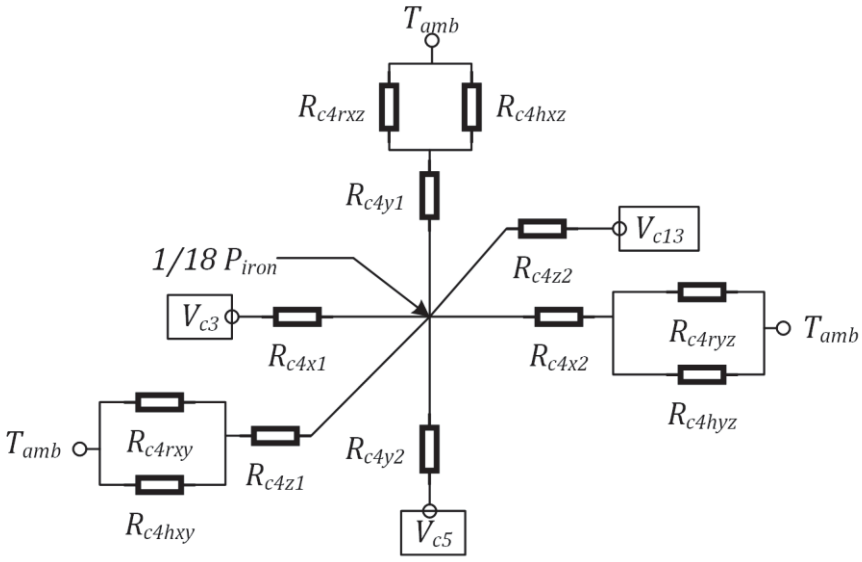

Figure 3.8 V_{c4} thermal resistances

Figure 3.8 shows the TRN of the V_{c4}, which involves a considerable number of elements, indicating a complex and hard to handle TRN of the modelled geometry, due to the massive number of resistances and connections. The heat source is connected to the middle point of the element, that for V_{c4} corresponds to iron loss (P_{iron}) divided by the 18 core's elements.

3.4.4 Winding Thermal Conductivity

Thermal resistances of the windings were obtained through the model developed in [4], as presented in Figure 3.9, which shows the winding structure and parameters. As the winding is a heterogenous element, it is necessary to obtain an average thermal conductivity. Commonly the electric conductor is a good heat conductor as well, whereas the electric insulator it is not a good heat conductor, e.g. copper conductivity is 1500 times higher than epoxy conductivity, therefore it is possible to consider the electric conductor as a perfect heat conductor.

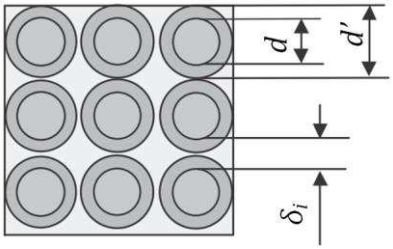

Figure 3.9 Winding structure (Adapted from [4])

The average conductivity for this type of winding is given by

$$k_{av} = k_i \left(\frac{d}{\delta_i} + \frac{\delta_i}{d'} \right) \tag{3.20}$$

where k_i is the thermal conductivity of the insulator material and the other parameters are introduced in Figure 3.9.

3.4.5 Results

With the thermal resistances and heat sources properly determined, the complete TRN can be solved by finding the equations related to temperature and solving it or using modern tools to solve electric circuits. In this work, the TRN solution was accomplished by using a circuit simulator, Multisim [58]. The thermal resistances of each volume element were calculated and connected accordingly to the contact of each element with the ambient and other elements, and the heat current related to the loss of each element was connected on the middle point of the volume element, as shown in Figure 3.8. The temperature results were obtained by placing voltage probes in the nodes of interest. Figure 3.10 shows the temperature spots presented in Table 3.2. Appendix B shows the TRN implemented in Multisim and its results for each element.

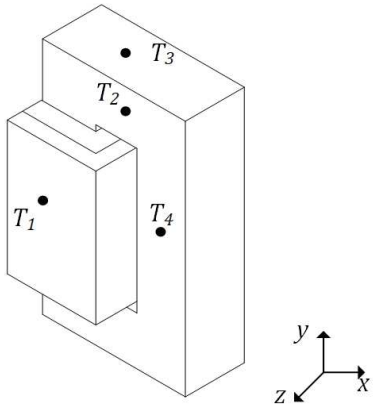

Figure 3.10 Transformer temperature spots

Table 3.2 TRN temperature results

Spot	Temperature (°C)
T_1	102
T_2	81.8
T_3	91.5
T_4	70.9

The higher temperature is spotted in the windings, as would be expected since they are the main heat source of the transformer. T_2 is higher than T_4 because it is closer to the windings than T_4. Regarding T_3 value, when compared with T_2 its higher value may be explained by the thermal conductivity of the core laminated steel since it is significantly lower in the *z*-direction, than the conductivity in *x* and *y*-direction. Difficulting the heat flow in the direction normal to the lamination, thus the heat flow in the core occurs majority on the *x* and *y*-direction. Alongwith, the core surface on plane *xz* is smaller than the core surface on plane *xy*, implying a lower heat transfer rate at plane *xz*.

3.5 Summary

In this chapter was discussed the main aspects of the thermal modelling by using thermal resistances network. This method is widely used due to its simplicity and fast solution, whereas the precision of the model relies on the effort spent into modelling details, discretization, and acquisition of thermal coefficients.

It was developed a TRN of a single-phase transformer, and its modelling process was detailed and explained. The results obtained from the TRN were presented and discussed.

Chapter 4

Numerical Modelling

4 Numerical Modelling

Numerical methods require high levels of computational power that was not easily available decades ago. With the advance of the digital computation, numerical methods became more feasible and popular. One of the most popular numerical methods is the finite element method (FEM), which was introduced in the early 1940s on the structural analysis field, and now it is established for all different analysis fields.

In this chapter it will be discussed the use of FEM in electric machines modeling, with focus in the electromagnetic and thermal fields. First, the concepts of FEM are introduced, and afterwards, the electromagnetic and thermal analyses are presented, and finally the electromagnetic and thermal coupled analysis is addressed.

The electromagnetic model is needed to provide the solution of the electromagnetic fields of the machine, which will determine its rated power, losses and other crucial aspects of the device. In the context of this work, the electromagnetic model is responsible to obtain the losses of the machine, that are determined by the magnetic flux density in soft ferromagnetic materials, i.e. the iron loss, and throught the density current in the conductors, the resistive loss.

The thermal model provides the temperature output of the machine due to its losses, being those the main input to its thermal model. Both the analytical and numerical thermal model considers the uniform heat generation within each part of the machine, by using a constant loss density. This assumption is a simplification since in practice, iron loss varies with the magnetic flux density along the iron volume. The electromagnetic and thermal coupled analysis overcome this limitation by using the electromagnetic model losses output as an input to the thermal model, that corresponds to a non-uniform heat generation accordingly to the magnetic flux density and current density distribution in the machine parts. Besides that, the coupled analysis uses the temperature output of the thermal model as input to the electromagnetic model, therefore considering the temperature dependency of the electromagnetic parameters.

The numerical modelling approach discussed during this chapter will be applied to the study case of a low power single-phase transformer, that is detailed and characterized in Appendix A. Also, its analytical thermal model was developed in section 3.4.

4.1 Finite Element Method

Finite element method (FEM) is a numeric technique developed to solve engineer problems related to physics phenomena described by differential equations. These elements are connected via nodes where the unknowns are to be determined. Algebraic approximations of the differential equations that describe the physics are applied to determine the element solution. The finite element equations are assembled into a set of algebraic equations, also the boundary conditions are imposed into this set of equations. At last the set of equations is solved, providing the solution of each node [59].

Three factors are important to FEM, differential equations, boundary conditions, and mesh geometry. Differential equations and boundary conditions are related to the physic phenomena properties, such as the differential equation of the heat conduction and the ambient temperature for a heat transfer problem. The geometry is the domain where the physics phenomena are occurring, it is divided into finite elements, and these finite elements can have different shapes (see Figure 4.1), a set of finite elements is called mesh. So the meshing process needs to be done carefully to discretize the geometry into several elements with appropriate shape, aiming the desirable precision with a reasonable computational cost.

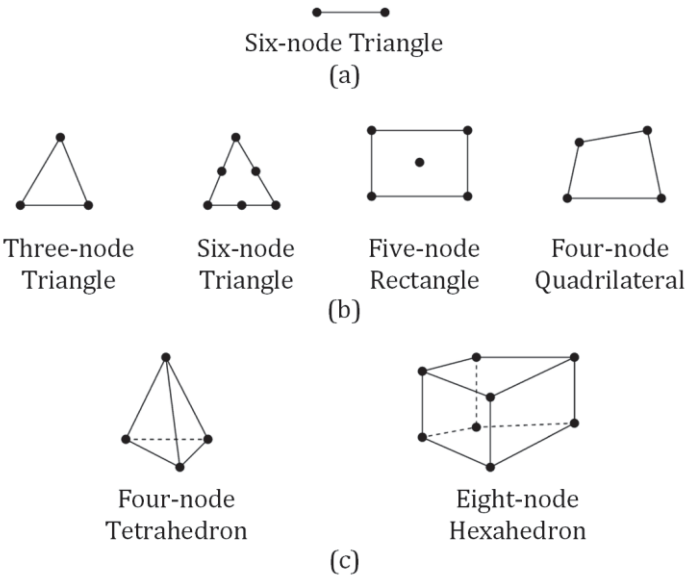

Figure 4.1 Typical finite elements: (a) One-dimensional, (b) two-dimensional, (c) three-dimensional. (Adapted from [60]*).*

The FEM is capable to solve 2D and 3D problems, therefore it is necessary to choose which geometry, 2D or 3D analysis, is more suitable for the model. The 2D geometry should be used in situations where variables under analysis do not change in one

direction, for instance, the magnetic flux densityvariation can be ignored on the direction normal to the lamination of a laminated electric steel. Also in situations where the heat conduction in one direction can be ignored, and the convection and radiation of the surfaces on that direction can be neglcted, 2D analysis may be condicted. Thus, the 3D geometry should be used in situations where all directions must be considered, which increases the computational weight of the solution, but corresponds to a more precise solution since the modelled electric machine corresponds to a 3D geometry.

FEM is implemented on a variety of software, allowing the exploitation of the tool without diving into the mathematical formulation of the method, but rather focusing on the knowledge of the physics phenomena, and being able to analyse correctly the FEM solution outputs. Therefore, the objective of this work is not to develop a FEM but use the FEM tools available on the market. Using FEM to study or analyse a phenomenon is called Finite Element Analysis (FEA), this is a powerful tool to quickly solve physic phenomena problems, helping engineers in several areas, such as the design process of a machine without having the requirement of building various prototypes.

4.2 Electromagnetic Finite Element Analysis

Electromagnetic phenomena are described by Maxwell's equations, being the electromagnetic FEA based on their differential form. Several studies regarding the electromagnetic model of electric machines were done using FEA, one of the main topics of these researches is the loss prediction and its mitigation. 3D FEA simulation is performed in [61] to study the losses and the electromagnetic field of a 90 VA transformer, in a similar way, [62] studies the iron loss of a 25 kVA distribution transformer under non-sinusoidal voltage, which is important due to the nowadays high usage of power electronics with their non-sinusoidal current waveform, causing distortions on the system supply. Reference [63] recommends the utilization of FEA to obtain accurate local electromagnetic field information to calculate iron loss.

Electromagnetic FEA is also important to explore the design efficiency of electric machines, [64] uses the FEA simulation to compare two design choices of a permanent magnet synchronous motor (PMSM). Whereas [65] investigate the impact manufacturing tolerance of permanent magnets on PMSM. It is also possible to analyse the electromagnetic fields and losses of electric machines with faults, such as [66] does on induction motors with broken bars. FEA is a powerful tool which gives a lot of information

on the electromagnetic field in the machine, allowing the user to explore a variety of applications.

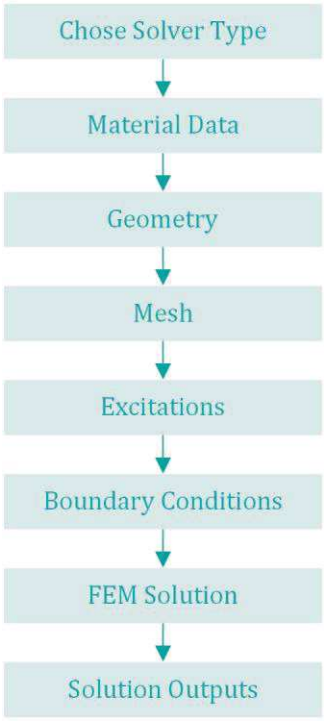

Figure 4.2 Electromagnetic FEA flowchart.

Figure 4.2 shows a flowchart of the generic setup of an electromagnetic FEA simulation. The first step to solve any problem is to identify which outputs are needed and which inputs are required. The geometry of an electric machine is 3D, thus for a more accurate model the 3D geometry should be used, although 2D solutions are suitable for situations where the physical phenomenon in one direction can be ignored.

Material data of the components are important to enhance the constitutive relations with accuracy, which may be complicated especially when the materials are nonlinear, anisotropic and inhomogeneous, like the iron core of electrical machines. The minimum data required for soft ferromagnetic materials is the *B-H* and specific loss curves, while for materials used in electrical circuits, the electric conductivity is mandatory.

To improve the performance of the FEM different solvers were developed, which were obtained by defining some of the field characteristics, e.g. magnetostatic solver the magnetic field is only produced by constant current flow or permanent magnets, this field characteristic specification allows a more efficient solver. As each solver is developed to fulfil a purpose it is important to read the software documentation to choose the solver type that suits the user application.

The meshing step is where the geometry is divided into finite elements, and it is necessary to pay attention to this step, a more refined mesh will have more elements, hence more calculations and more time to obtain the solution. FEA software assists this process by informing mesh metrics, allowing the user to evaluate if the mesh gives the desired level of discretization.

Excitations are chosen according to the solver type and application, they can be DC sources, permanent magnets or time-dependent sources. In more advanced software packages it is possible to use power electronics allowing to simulate complex working conditions.

The boundary conditions are defined accordingly to the physics phenomena, and the characteristics of the device, the appropriate use of the boundary conditions is necessary to model the physics phenomena along the domain boundary correctly. Thus, each solver type make available the boundary conditions accordingly to the physics phenomena. Commonly, are used two boundaries conditions, the Neumann conditions where it defines the value of the solution derivative on the domain boundary, and the Dirichlet conditions, which specifies the solution value along the domain boundary.

If the steps above were properly done, now it is possible to run the FEM and analyse its solution. Now begins the analysis step, where the user needs to use his phenomena knowledge to evaluate the FEM results. Without the proper knowledge of the physical phenomena, the FEM solution is just a set of numbers, thus the final task of the user is to transform this set of numbers into tangible information.

4.2.1 Numerical Electromagnetic Modelling of a Low Power Transformer

In the context of this work, the electromagnetic model is developed to obtain the electromagnetic losses of the machine and their non-uniform distribution. Therefore, the electromagnetic model of the transformer was developed to match the rated working conditions, hence the resistive and iron losses under the rated working conditions. The electromagnetic FEA was developed by using the Ansys Maxwell 2019 R3 [67] software package. Appendix A presents more details about the transformer.

The interest of this work is to establish the relation between heat generation and its management in electric machines. Therefore the doutput wanted is the losses distribution on the transformer, so it is necessary to use a 3D geometry (Figure 4.3) to

obtain the distribution of the iron loss on the core's volume and the resistive loss in the windings' volume.

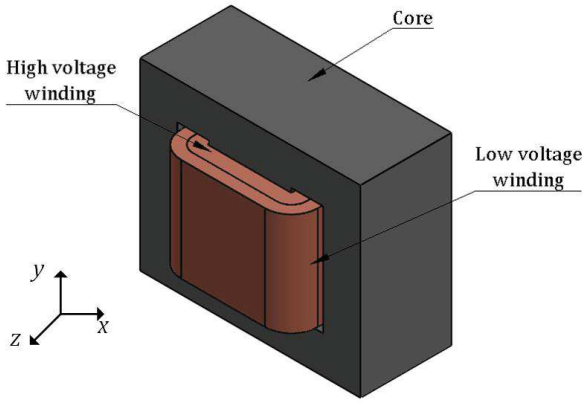

Figure 4.3 Transformer geometry.

The material data required to model the transformer are the core's *B-H* curve and specific loss, and the electric conductivity of the windings. Figure 4.4 presents the core's material data, that was adapted from one manufacturer [68]. The windings are made of round wire impregnated copper, which has the conductivity of 58×10^6 S/m [4].

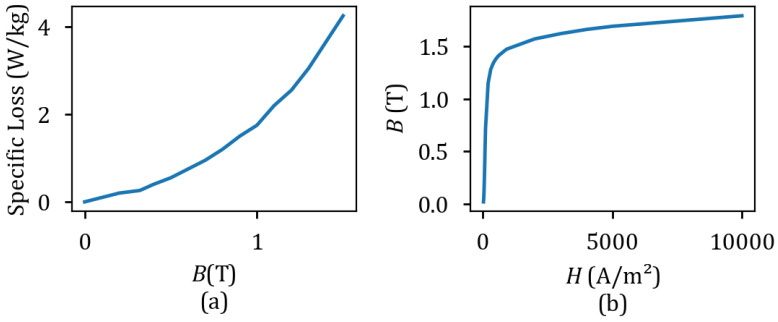

Figure 4.4 Laminated steel properties: specific loss (a), B-H curve (b).

Next step is to choose the solver type: the magnetostatic solver is capable to calculate only the resistive loss; to obtain both losses, resistive and iron losses, the transient solver is required in order to simulate the magnetic flux variation[69]. Since it is a transient simulation, it is necessary to specify the time step and time of the simulation. The desired output is the losses, so the simulation needs to represent at least one complete period of the excitation cycle, which, according with the reated characteristics of the transformer, is 50 Hz or 20 ms.

The iron loss is obatained by the Ansys Maxwell built-in iron loss calculator that is based on the Bertotti model [35], that was addressed in section 2.1.2. The coefficients used in the iron loss model are automatically determined by the software, after providing

the specific loss curve (Figure 4.4 (a)), the electric conductivity of the electrical steel sheet, and its thickness, that was defined as 2×10^6 S m and 0.5 mm, respectively.

Figure 4.5 shows the magnetization curve of a soft ferromagnetic material, that expresses the relation between *B* and *H*. In the point *a* the magnetic domains are randomly oriented which results in a zero magnetization. As the external magnetic field increases the magnetic domains will follow the orientation of the field, increasing magnetic flux density. The path *a* – *b* is called the initial magnetization curve. As *H* decreases *B* will also decrease, but it will not follow the initial curve (*b* – *a*), it will follow the path *b* – *c*. This characteristic of not following the initial path of the magnetization is called hysteresis, and the magnetization path of the ferromagnetic material after the first magnetization (*b* – *c* – *d* – *e* – *b*), is called hystereis loop.

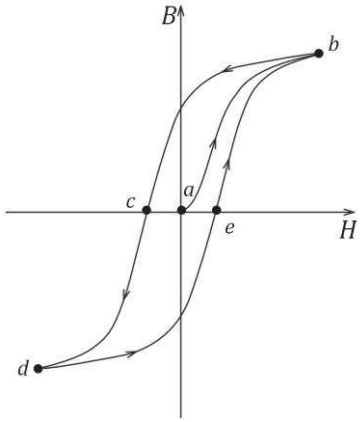

Figure 4.5 Magnetization curve of a soft ferromagnetic material (Adapted from [70]*)*

As the hysteresis loop is only established after the initial magnetization curve, the iron loss must be considered after the intial magnetization curve, which occurs in the first half period of the excitation. For the excitation applied to the transformer the time taken to occur the first magnetization is 10 ms, thus the simulation must cover at least 10 ms plus one complete period of the excitation. So, the time defined for the solver is 30 ms with a time step of 0.5 ms.

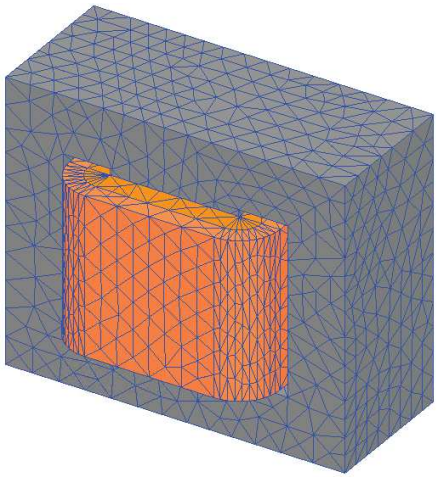

Figure 4.6 Transformer electromagnetic FEA: mesh.

Figure 4.6 shows the transformer's mesh, since the 3D transients simulation is demanding on computational resources the mesh size was adjusted by the software parameters, conciliating the solution precision and computational cost.

The excitations of the transformer were done by firstly setting up the number of turns of each winding and its current flowing direction since it is a shell type transformer, the directions of the windings are opposite. The electromagnetic models the rated working conditions of the transformer, because in these conditions the nominal current is flowing through the windings and the magnetic flux density on the core corresponds to the rated voltage, granting that both losses are addressed in their rated values. To simulate the rated working conditions, an external circuit excites the high voltage winding with its rated voltage and connects a resistive load to the low voltage winding which imposes the rated currents to the windings.

It was applied an insulating boundary condition between the windings, which models the insulation material between them, this condition defines that the current cannot cross the boundary, H is tangential to the boundary and the flux cannot cross it [69]. Since the interest of the analysis is in the electromagnetic field of the transformer, it was applied a Naumann boundary condition on the transformer's external boundaries, where it defines the H is tangential and the flux cannot cross the boundary. Thus, it does not calculate the magnetic field on the ambient around the transformer, isolating the transformer from the ambient.

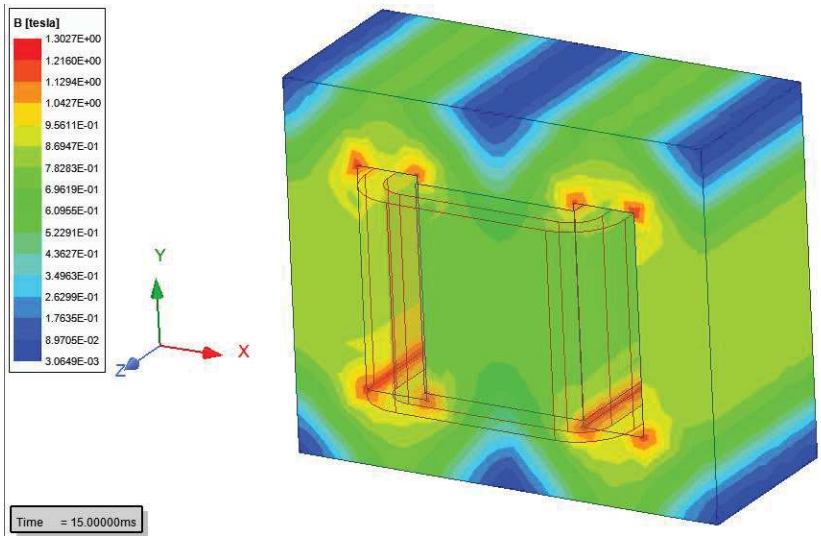

Figure 4.7 Transformer electromagnetic FEA: magnetic flux density.

With all the setup properly done it is possible to run the solver and analyse the solution. Figure 4.7 shows the magnetic field flux density in the transformer core at 15 ms, the maximum value is 1.30 T, which is far from the saturation level of the ferromagnetic material, and the high values occurs only in the edges close to windings.

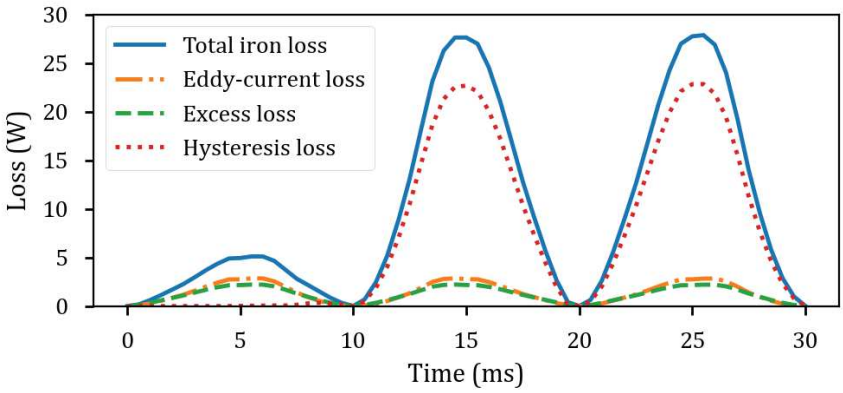

Figure 4.8 Transformer electromagnetic FEA: iron loss.

Figure 4.8 displays the iron loss of the core during the simulation, is possible to see the difference on the iron loss during the first magnetization curve, and after the hysteresis loop establishment, the average iron loss between 10 ms and 30 ms is 13.78 W. Since, ANSYS Maxwell iron loss calculation is based on the loss separation approach, is possible to observe the contribution of each portion of iron losses (hysteresis, eddy-current, excess eddy-current) to the total iron loss. And the average resistive loss of the windings at ambient temperature is 44.12 W.

4.3 Thermal Finite Element Analysis

The heat transfer phenomena used in thermal FEA were previously described in chapter 2. FEA allows high levels of discretization granting accurate solutions regarding the heat transfer through conduction, which provides an accurate temperature distribution in the machine's geometry. Reference [71] exploits this FEA advantage to investigate local temperatures in the tank of a power transformer, in a similar way [24] studies the thermal impact on the bushings of a transformer. The determination of the convection heat transfer coefficient is based on the same relations used in the TRN modelling, although in TRN the coefficient is considered as a constant value, whereas in FEA the implementation of the temperature dependency of the convection and radiation coefficient is straightforward. Figure 4.9 shows a flowchart of the thermal FEA model.

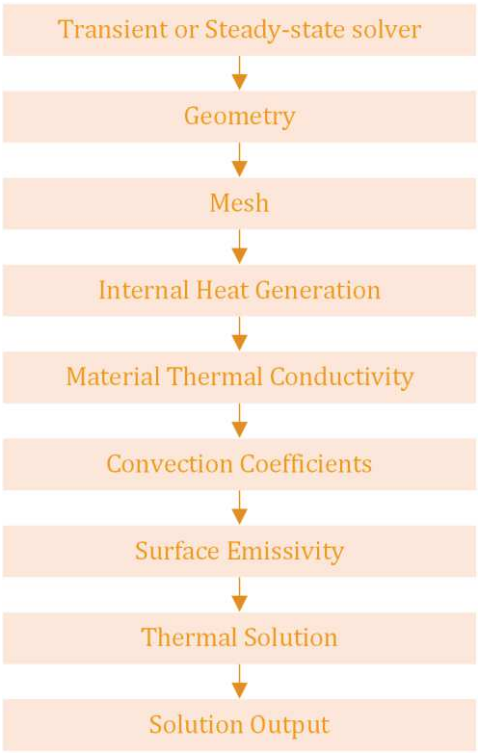

Figure 4.9 Thermal FEA flowchart.

Typically the thermal steady-state of the machine is the required state, because it reflects the stable temperatures on working conditions, though, the transient solution is important to see how long the machine takes to heat up and cools down, which can be crucial for applications that require several starts. Reference [25] is an example where the thermal transient solution is used to investigate the temperatures of an induction motor during the starting process.

Since the losses are generated inside of the machines they are treated as internal heat generation, which are modelled by a power density (W/m^3) that can be distributed uniformly within the geometry, or in a way that better resembles the real heat generation. Next step is to determine which surfaces will perform convection and their respective convection coefficients. For the radiation is the same process as the convection, with the difference that instead of convection coefficients, is necessary to input the emissivity of the surface. The thermal conductivity of the machine materials will define the heat conduction, for a anisotropic material is necessary to input the thermal conductivity of each direction. Finally, with the heat distribution defined and the heat transfer mechanisms characterized, it is possible to run the thermal FEM solution and procedure its analysis.

4.3.1 Numerical Thermal Modelling of a Low Power Transformer

The thermal FEA simulation of the transformer characterized in Appendix A was performed, by considering an uniform distribution of the losses on their respective parts. Ansys Mechanical 2019 R3 [72] software package was used to perform the thermal FEA model.

The 3D geometry is the same used in the electromagnetic FEA (see Figure 4.3). Since the desired output is the steady-state temperature distribution of the transformer, it is possible to have a more refined mesh without having a significant impact on the solution time. Table 4.1 shows the power density values applied to the model.

Table 4.1 Power density distribution

Geometry	Loss (W)	Power density (W/m^3)
Core	13	1.35×10^4
Low voltage winding	20.26	1.59×10^5
High voltage winding	20.34	1.07×10^5

Figure 4.10 shows the surfaces that will perform convection and radiation heat transfer with the corresponding coefficient. As the surfaces for radiation and convection are the same, the label pattern of the radiation heat transfer coefficient follows the same numbering of the convection coefficient, only the subscript *r* is added, e.g. h_{rc1}, h_{rw2}, whereas subscripts *c* and *w* correspond to core and winding surfaces, respectively. For aesthetic reasons, the winding surface facing down (plane *xz*) is omitted, its corresponding coefficient is h_{w3}.

In contrast to the TRN, where the convection coefficient is considered a constant value, the convection coefficients are inserted in Ansys Mechanical as a temperature surface function, calculating more accurately the convection heat transfer. The convection coefficients were defined by the same empirical relations used in the analytical model. Figure 4.11 shows one of the coefficients used. The temperature also impacts in the thermal conductivity of the materials, however for most cases it can be used a constant average thermal conductivity. In this work the thermal conductivity is considered constant, due to the unavailability of the parameters necessary to consider this temperature dependency, and the thermal conductivity of resembling materials presents slightly variation for the temperature rise occurring on the transformer.

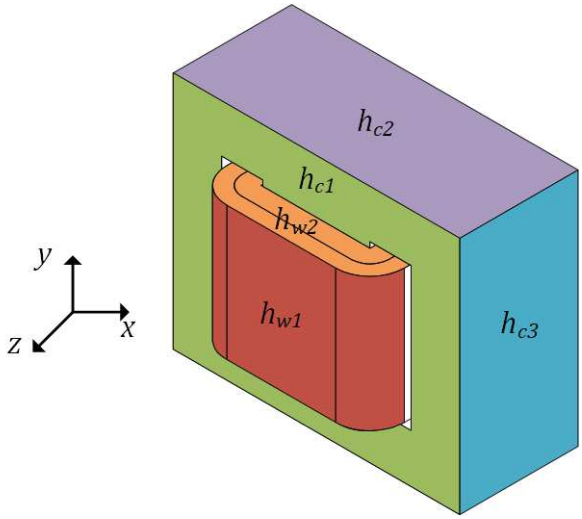

Figure 4.10 Transformer thermal FEA: Convection and radiation surfaces.

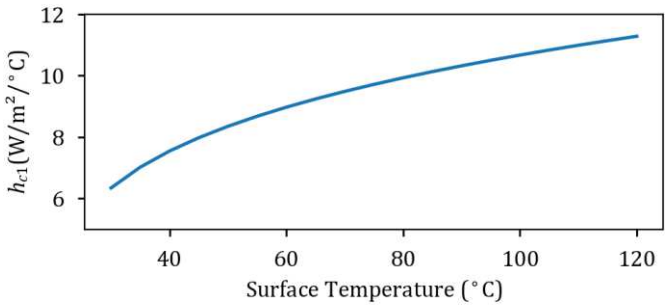

Figure 4.11 Transformer thermal FEA: convection coefficient h_{c1}.

The windings surfaces that are wrapped in a black electrical tape has the emissivity value of 0.9, and the other surfaces emissivity value is 0.3, and the thermal conductivity of the materials is summarized in Table 4.2 [4].

Table 4.2 Thermal conductivities.

Material	k_x (W/°C/m)	k_y (W/°C/m)	k_z (W/°C/m)
Core laminated steel	31	31	0.6
Low voltage winding	7.04	7.04	7.04
High voltage winding	5.95	5.95	5.95

Figure 4.12 shows the temperature distribution output, it is possible to see that the higher temperature spots are on the windings, and the surfaces closer to the windings. It is interest to analyse the temperature gradient on *z*-direction due to the low thermal conductivity of the laminated steel, if the thermal conductivity in *z*-direction was higher the heat flow in this direction would increase, and consequently the temperature values on plane *xz* would be smaller. Additionally, it is possible to observe that the temperature distribution is symmetric on the planes illustrated in Figure 3.5, which supports the boundary condition applied to the TRN model (section 3.4.3), where it was considered that there is no heat transfer between the modelled portion of the transformer and its symmetry counterpart, due to the minimal temperature difference and small heat path between the modelled portion and its symmetry counterpart.

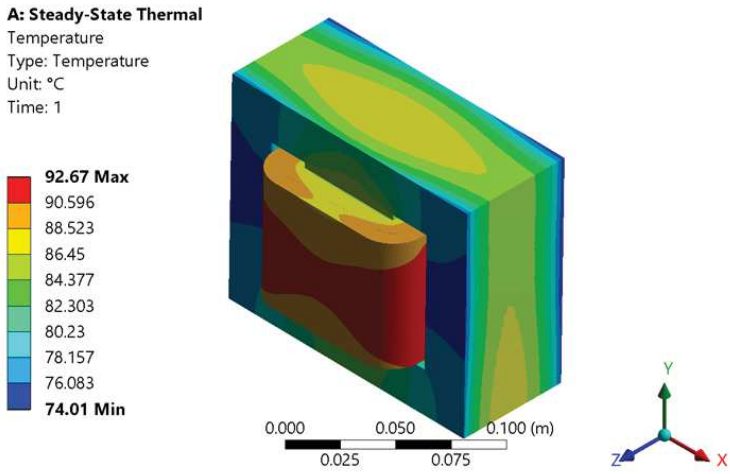

Figure 4.12 Transformer thermal FEA: temperature distribution.

The total heat flux presented in Figure 4.13, shows the paths of the heat exchange occurring from the surfaces to the ambient and also the heat flowing from the windings to the core, and from the core to the ambient. Thus, the core operates as a heat sink for the heat generated in the windings.

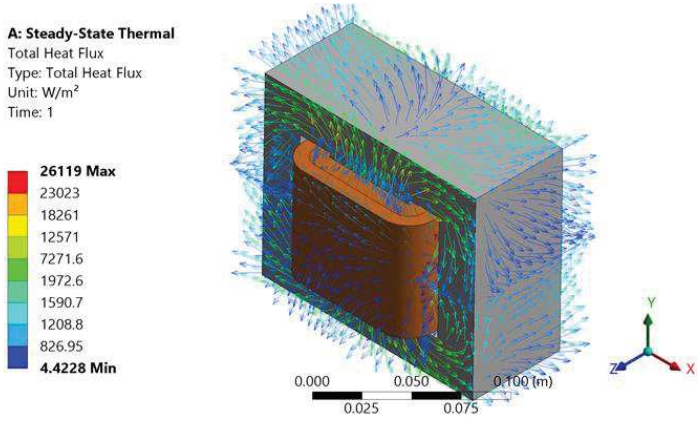

Figure 4.13 Transformer thermal FEA: heat flux.

4.4 Coupled Electromagnetic and Thermal Finite Element Analysis

The coupled analysis allows a complete interaction between the electromagnetic and thermal fields. That is a natural demand to improve the design process of electric machines to fulfil the nowadays requirements of power density and efficiency. The losses obtained by the electromagnetic model are used as the heat generation input in the thermal model, that will calculate the temperature distribution of the machine, and the temperature output of the thermal model is used as input to the electromagnetic model, in order to calculate the losses considering the temperature impact on the electromagnetic parameters. This interaction between the electromagnetic and thermal model runs iteratively until the variation of temperature between the two last iterations is lower than a defined threshold, meaning that the temperature and losses variation is minimal. Differently to the thermal model developed in section 4.3.1, where it is considered a uniform heat generation, the coupled model considers the heat generation distribution as the losses distribution output of the electromagnetic model.

The FEA regarding only one physics field was introduced in the previous sections. So, the objective of this section is to couple the analyses that were previously treated separately, therefore granting a complete interaction between the electromagnetic and thermal fields. The use of coupled analysis is a natural demand to improve the design process of electric machines to fulfil the nowadays requirements of power density and efficiency.

The coupled analysis approach allows the evaluation of the electromagnetic model according to the temperature change. Material properties from the magnetic and electric circuits vary non linearly with temperature, and for this reason, the thermal model output

can be crucial to evaluate the electromagnetic performance of the electric machines. The temperature rise increases the resistive loss and also brings the risk of demagnetization For instance, if the machine uses permanent magnets in its excitation system, for an operating temperature of 100°C, the magnetic flux may be reduced till 20% when compared with the magnetic flux at room temperature [2], which impacts directly on the machine performance.

This approach is a handful in the machine design process, allowing the engineers to evaluate the design choices impact in a wider view. Such as in [73], where the design process of a medium frequency power transformer is done by utilizing FEA and the validation was achieved by building the prototype based on the FEA project. Similarly, [74] uses the FEA coupling to investigate different rotor structures of a synchronous generator, observing that a claw pole rotor is more thermally efficient than a salient pole rotor.

The coupled methodology proposed in this work is intended to be used as part of the design process of an electric machine, or it can be useful to evaluate the machine performance in operating conditions that differ from the rated ones. An example is the derating of the machine in ambient temperature or altitude different from the ones specified for the rated quantities may be more precise, if assisted with an electromagnetic and thermal coupled approach.

Figure 4.14 summarizes the proposed coupled methodology. Most of the flowchart elements were explained on the previous sections, thus this flowchart establishes the link between the electromagnetic and thermal analysis. A magnetostatic solution is present in this flowchart, since it is a simple and quick solution that allows the evaluation of some features, such as iron saturation, hence guiding to some model changes e.g. geometries, ferromagnetic material requirements, excitations sources. The generated losses resulted from the electromagnetic FEA solution are used as heat generation in the thermal FEA. This interaction between the solutions, grants the heat generation be closer as possible to the real loss distribution. Due to the temperature change, material properties such as electric conductivity will change, thus the electromagnetic solution needs to be updated considering the components new temperatures. This iterative process runs until the temperature difference between the current interaction and the previous minor than δ, meaning that the temperatures and losses are stable.

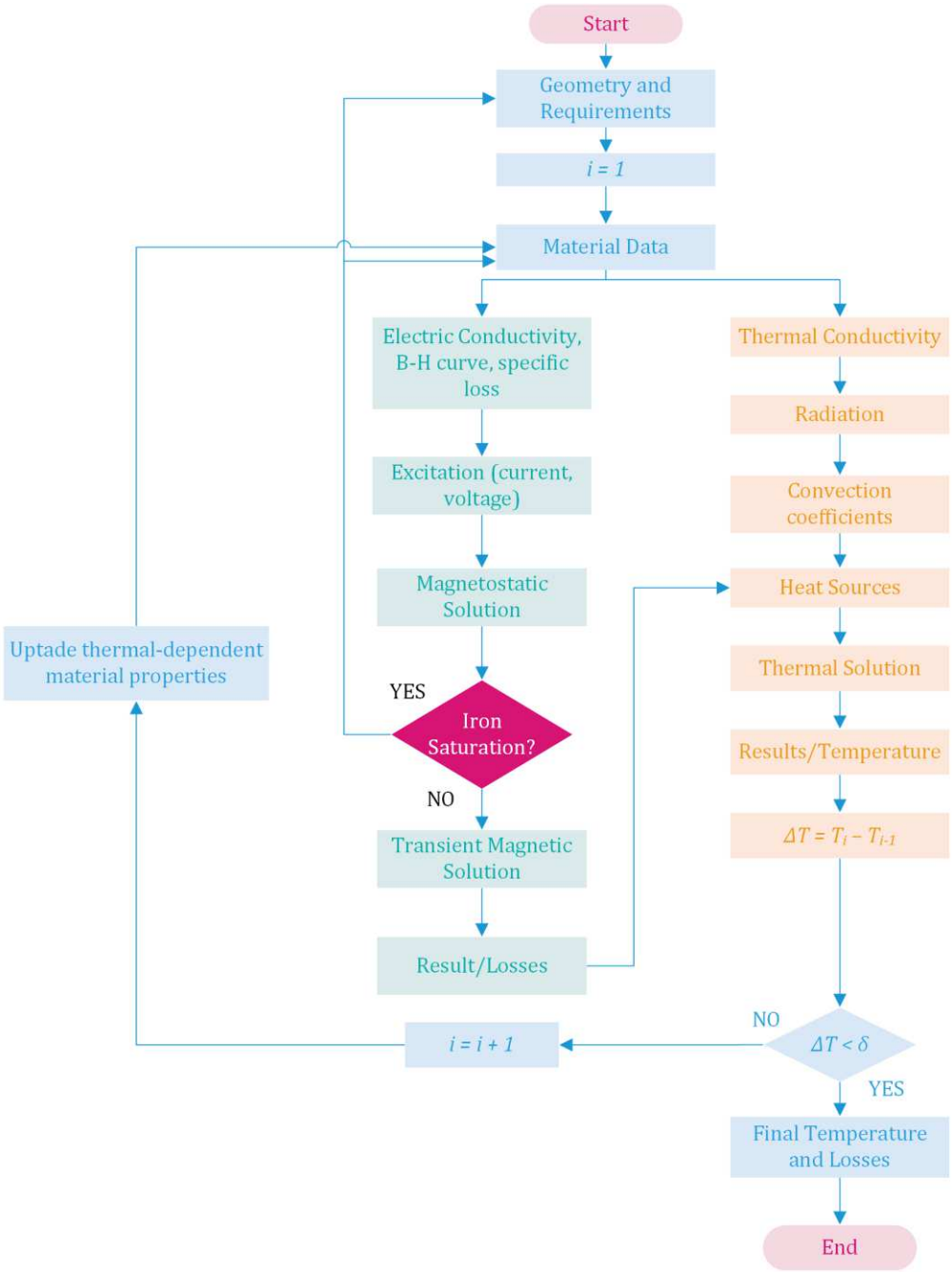

Figure 4.14 Electromagnetic and thermal coupled analysis flowchart.

4.4.1 Numerical Coupled Modelling of a Low Power Transformer

By using Ansys Workbench 2019 R3 [75] an electromagnetic and thermal coupled analysis of the single-phase transformer was made. The coupled analysis was set up by importing the losses from Ansys Maxwell (electromagnetic FEA) into the Ansys Mechanical (thermal FEA) and exporting the temperature distribution to the Ansys Maxwell, and the thermal modifier was enabled in the electromagnetic FEA. This interaction between the losses and the temperature was only applied to the resistive loss, where the copper electric conductivity is defined as

$$\sigma_{cu} = \sigma_{20} \frac{1}{1 + \alpha(T - 20)} \tag{4.1}$$

Where σ_{20} is the conductivity of the copper at 20 °C, that is equal to 58×10^6 S/m, and α is the copper thermal resistivity coefficient, which is equal to 3.93×10^{-3} °C^{-1} [76].

The electromagnetic and thermal FEA used are the models developed in section 4.2.1 and 4.3.1, respectively, with the difference that the internal heat generation is now obtained from the Ansys Maxwell solution. Therefore, this simulation corresponds to the transformer on its rated working conditions. In Figure 4.15 is possible to see the evolution of the transformer losses along with the iterations. The resistive losses increased 32.82% between the first iteration and the last, is possible to see that in the last three iterations the losses increase were minimal.

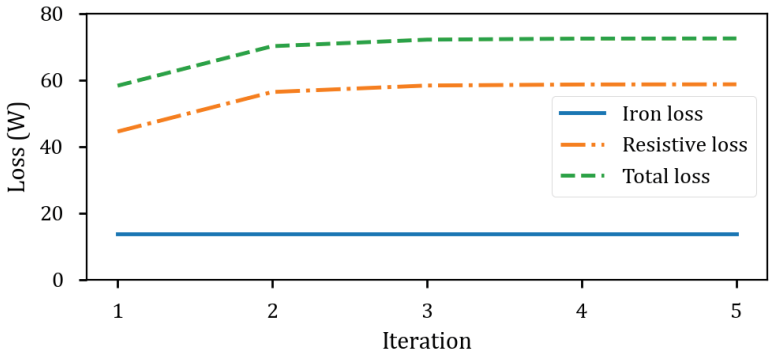

Figure 4.15 Transformer coupled FEA: loss evolution.

The temperature rise is shown in Figure 4.16, which follows the same aspect of the losses, in the initial iterations there is significant increase and in the last iterations, the temperature rise is minimal. The average temperature of the model increased in 12.48°C between the first and the last iteration, which is a significant temperature difference that would be ignored if the coupled analysis was not applied.

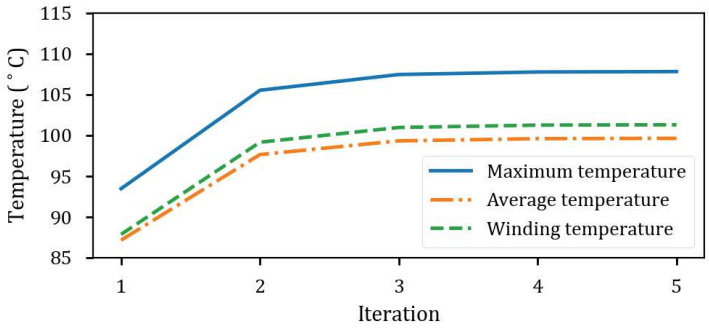

Figure 4.16 Transformer coupled FEA: temperature evolution.

It is possible to see that for this case, was not needed to run several iterations, with three iterations the simulation results were already stable. Were expected this low number of iterations since only the resistive loss was considered temperature-dependent.

This analysis was done to simulate the transformer behaviour at electric rated conditions, and under normal conditions of temperature and pressure. However, it is possible to adjust the coupled FEA project to simulate different electric and ambient conditions e.g. underload, overload, high ambient temperature, thin air. Thus, the coupled analysis can assist the optimization and derating of the transformer design for applications with such conditions.

4.5 Summary

In this chapter was discussed the numerical modelling of electric machines using the FEA, which is a tool that was introduced decades ago in the structural analysis field, and nowadays is developed for a variety of physics fields. FEA is a powerful tool that facilitates the coupling of different physics fields, which can be crucial for the design process of modern applications. Within the electric machine context, the electromagnetic and thermal FEA and their coupling were addressed. And to demonstrate the methodology presented for the numerical modelling, it was developed the numerical model for a single-phase transformer.

Chapter 5

Results and Discussion

5 Results and Discussion

In the course of this work it was discussed different approaches to model electric machines. These approaches were applied to a low power single-phase transformer. The objective of this chapter is to summarize, discuss, compare, and validate the results obtained from the models. First, the experimental procedure and measurements of the transformer are presented, thereafter, the results from the models are summarized, compared, and discussed.

5.1 Experimental Results

To obtain the experimental losses of the transformer, the device was submitted to two tests, these tests were initiated with the transformer at ambient temperature (20 °C), as these tests occur in a short period, the temperature rise of the machine can be ignored. Appendix A contains more details about the performed tests. Therefore, the measured resistive loss at 20 °C was 49.6 W, and the measured iron loss at 20 °C was 13 W.

The desired approach to measuring the temperature of the transformer was to use the PT 100 temperature sensor in concerned spots of the transformer. Although, due to the COVID-19 pandemic, it was not possible to perform this procedure. In order to still have experimental validation, a student under Prof. Ângela Ferreira supervision during his internship period in IPB, which occurred previous to this work, obtained the experimental thermal data used in this work.

The temperature monitoring of the transformer was accomplished by using an infrared thermography camera. The camera absorbs the infrared radiation emitted by the body, and by using the Stefan-Boltzman's law the body temperature is obtained [70]. Its use allows measuring the surfaces temperatures of the device without contact. Thus, it is not possible to measure the temperature of spots that are not in the device surface, such as the temperature between the windings.

In the laboratory at the ambient temperature of 20 °C, the transformer was submitted to the rated working condition. Thus, the high voltage winding was excited by the rated voltage, and on the low voltage winding, a resistive load was connected.. Thermal behaviour of the machine was supervised through an infrared camera. Figure 5.1 shows the thermal steady-state of the transformer. The infrared camera was configured with the emissivity of the black insulation tape of the windings. The obtained images are

useful to evaluate the temperature gradient and the thermal steady state condition, not being able to evaluate absolute temperatures of the surfaces.

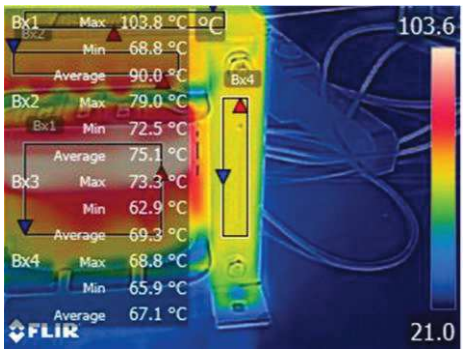

Figure 5.1 Thermal image of the transformer after 200 minutes.

As the thermal images are not reliable to obtain absolute temperatures, the temperature of the windings was measured by using the procedurement recommended by the IEC 60034 [77]. Which consists in measuring the winding resistance at the known initial temperature and measuring the winding resistance after the temperature rise, after these measurements, the temperature of the winding is determined by

$$T_f = \frac{R_f}{R_i}(T_i + \lambda) - \lambda \tag{5.1}$$

where R_f is the winding resistance at the final temperature, R_i the winding resistance at the initial temperature T_i, and λ is the reciprocal of the temperature coefficient of resistance at 0 °C of the conductor material, that for copper is 235 and 225 for aluminium. Table 5.1 shows the results obtained from the IEC method, with the values of the resistances of the windings at steady-state temperature, the resistive loss can be calculated considering the temperature rise in the windings, the skin-effect is ignored in this case since the skin depth of the copper is higher than the diameter of the winding's wire.

Table 5.1 Windings temperature measurement (IEC 60034).

	R_i (Ω)	R_f (Ω)	T_f (°C)	Resistive Loss @T_f (W)
Low voltage winding	0.4	0.52	96.5	36.26
High voltage winding	1.0	1.3	96.5	25.20

5.2 Summary of the Models Results and Discussion

5.2.1 Losses Results

In section 4.2.1 the electromagnetic FEA model of the transformer was developed with the objective to calculate the losses of the machine. With losses measurements of the transformer, it is possible to evaluate the accuracy of the loss prediction of the model. Table 5.2 shows the losses measured and calculated, and the relative error between them. These results are related to losses of the transformer at ambient temperature of 20 °C.

Table 5.2 Transformer losses: experimental and FEA.

	Resistive Loss (W)	Iron Loss (W)
FEA	44.12	13.78
Experimental	49.60	13.00
Error (%)	11.05	6.00

The results obtained from the model are in agreement with the experimental measures. The errors presented by the model may be related to some uncertainty in data of the active materials and dimensions of the physical transformer, e.g., number of turns of each winding, specifications of the ferromagnetic material used on the core. As explained in section 2.1.2 the prediction of the iron loss is very difficult due to the complexity of the phenomena involved. The advantage of using an FEA model is that the iron loss is calculated for each element, considering the non-uniform flux density on the core. Given these aspects, the results presented by the model are acceptable.

5.2.2 Temperature Results

The analytical and numerical thermal model of the transformer was developed in section 3.4 and 4.3.1, respectively. Both methods use the losses obtained by the experimental test at 20 °C, considering a uniform distribution of the iron loss on the core, and the resistive loss on the windings. Figure 5.2 shows the temperature spots used to compare the temperature results of the analytical and numerical model.

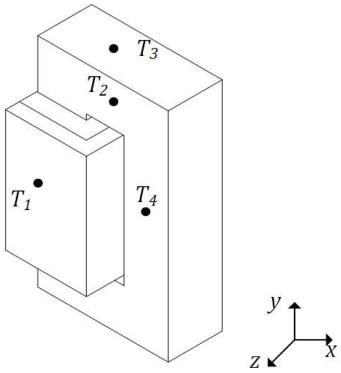

Figure 5.2 Transformer temperature spots

Table 5.3 shows the results from both models and their difference. The temperature spots T_2 and T_3 presented a small difference between the models, whereas the spots T_1 and T_4 presented a temperature difference of about 10%. The discretization levels between the models are very different, which can be related to the temperature difference between the models. The TRN approach used a total of 26 volume elements to model ¼ of the transformer, whereas the FEA used 15821 elements to model it entirely. Even with this discrepancy between the discretization level, the results are similar, although this may not be the case for machines with complex geometries. Another factor that impacts the results difference is related to the convection coefficients. The model used in TRN considered the convection coefficient constant. In contrast, the numerical approach considered its variation with the surface temperature, which leads to a more precise convection heat transfer calculation in the FEA method.

Table 5.3 Temperature results from the transformer thermal models

Spot	TRN (°C)	FEA (°C)	Difference (%)
T_1	102	91.52	11.45
T_2	81.8	81.92	-0.14
T_3	91.5	88.01	3.97
T_4	70.9	78.04	-9.14

In section 4.4.1, it was developed the numerical coupled electromagnetic and thermal model of the transformer, where the models run iteratively, considering the temperature dependency on the loss calculation and the non-uniform heat generation. When the solution reaches the established threshold of the temperature difference between the two last iterations, the temperature output of the coupled model corresponds to the transformer at its steady-state condition. Therefore, the windings' temperature output of the model on the last iteration can be compared to the

temperatures measured through the IEC 60034 method after the transformer reached a steady-state condition.

The results of the analytical and numerical thermal model previously shown, are obtained considering the losses of the transformer at ambient temperature. Thus, they can not be compared to the temperature measured on steady-state conditions. So, the resistive loss of the models was calculated and updated considering the windings' resistance at steady-state temperature. Table 5.1 shows the resistive loss at the steady-state temperature.

Table 5.4 shows the steady-state temperature of the windings, that was obtained experimentally through the IEC 60034 method, and the temperature of the models corresponds to the average temperature of the windings. The TRN model presented an error of about 20% in relation to the experimental value, whereas the FEA and coupled FEA models presented errors of around 7%.

Table 5.4 Temperature of the windings at steady-state

Location	Experimental (IEC 60034) (°C)	TRN (°C)	TRN Error (%)	FEA (°C)	FEA Error (%)	Coupled FEA (°C)	Coupled FEA Error (%)
Low voltage winding	96.5	115.6	19.51	102.89	6.62	103.57	7.3
High voltage winding	96.5	116.17	20.38	101.95	5.65	102.91	6.64

Table 5.5 shows the temperature results of the models at the steady-state condition regarding the temperature spots indicated by Figure 5.2, and the temperature difference between the models. Reiterating, that there is no experimental value for these temperature spots, because the infrared camera does not provide reliable measurements of the absolute temperature on the spots.

Table 5.5 Trasformer temperature results: TRN, FEA, and coupled FEA

Location	TRN (°C)	FEA (°C)	Coupled FEA (°C)	Temperature Difference (%)		
				TRN vs FEA	TRN vs Coupled FEA	FEA vs Coupled FEA
T_1	115.00	101.32	101.27	13.50	13.56	0.05
T_2	89.20	88.27	88.13	1.05	1.21	0.16
T_3	100.00	96.62	100.41	3.50	-0.41	-3.77
T_4	76.70	84.93	85.01	-9.69	-9.79	-0.09

The results show that the FEA and coupled FEA models presented results very similar results, the highest temperature difference between them occurs on spot T_3 where the FEA model resulted on a temperature 3.77% cooler than the coupled FEA. This small difference between the models is related to the losses used on the models. The thermal FEA uses the losses obtained experimentally, and the use of resistive loss at steady-state temperature was only possible due to the measurement of the windings' resistance at the steady-state temperature. While, the coupled model uses the losses obtained by the electromagnetic model, which are calculated automatically considering the non-uniform loss distribution and the temperature dependency of the materials. Thus, the coupled FEA model does not require the physical prototype to obtain the losses of the machine for different temperatures. And this is why the coupled model facilitates the design process of electric machines, without the need of a physical prototype is possible to simulate the multiphysics behaviour of the device, allowing to study design choices without the time and cost of building numerous prototypes.

The results from the TRN are very similar to the numerical methods on the temperature spots T_2 and T_3, while presented significant difference on spots T_1 and T_4. These results indicate that the higher level of discretization present on the numerical methods allowed better modelling of the heat paths on the windings. Indicating that the thermal resistances of the windings were overestimated. Besides that, the convection heat transfer is calculated more precisely on the numerical methods, considering the temperature of the surface on the value of the convection heat transfer coefficient.

With the results presented by Table 5.4 andTable 5.5, it is possible to draw some conclusions regarding the performance and improvements of the models. All models predicted a higher temperature on the windings than the ones obtained experimentally. Thus, it should be considered the use of experimental thermal coefficients of the actual

materials and fluid flow of the transformer, which would allow the models to better resemble the physical transformer.

5.3 Summary

The modelling approaches of electric machines discussed during this work were applied to a low power single-phase transformer, due to its simplicity and availability on the laboratory. This chapter summarized the results obtained from the developed models and confronted the theoretical results with experimental results obtained on the laboratory. The numerical models presented good performance, but the analytical thermal model presented significant error when compared to the experimental measurements. With the results presented allows identifying future improvements for the models, such as the characterization of the electromagnetic and thermal parameters of the actual materials present on the transformer. Also, the TRN results suggest an overestimation of the thermal resistance, especially on the windings, and should be considered a more refined calculation of the convection heat transfer.

Chapter 6

Conclusion

6 Conclusion

This work aimed at discussing the modelling process of electric machines focusing on the electromagnetic and thermal modelling. The classic design process of electric machines is focused on the electromagnetic design and overlooks the thermal design, relying on the use of empirical experience, especially for medium and small-sized machines. As a reaction to the modern requirements of electric machines applications, the thermal modelling of the electric machine has been receiving more attention in the past years.

The thermal model is achieved by an analytical and numerical approach. The analytical approach, TRN, discretizes the heat transfer phenomena into thermal resistances, similar to an electric circuit. Regarding the numerical model, it is obtained by FEA that is commonly used due to its high level of discretization granting a precise temperature distribution. Both methods were applied to model a low power transformer, where the FEA model presented better results on the prediction of the temperature of the windings when compared to experimental measurements. Results showed that the higher level of discretization present in the FEA model has a significant impact on the determination of the hot spots. Also, the FEA model has a straightforward implementation of the temperature dependency of the convection heat transfer coefficient, allowing to model more accurately the heat transfer through convection. The TRN model shows that despite being a simple analytical method, it can produce satisfactory results.

Electric machines temperature rise is caused by the device's losses, which are mainly electromagnetic losses, being divided into resistive loss and iron loss. The resistive loss is usually the principal heat source in electric machines, the electric resistance of the conductor is strongly dependent on its temperature, this relation is expressed by a simple equation, allowing a direct temperature dependency of the resistive loss. Whereas the iron loss modelling is a difficult challenge itself, having different approaches and formulations, therefore its thermal dependency it is not straightforward, though, is known that the iron loss reduces with the temperature rise. Also, the fundamentals of heat transfer were established, which allowed the understanding of the main aspects related to heat removal mechanisms.

A methodology for coupling the electromagnetic and thermal analyses was proposed to handle the multiphysics characteristics of electric machines. By applying the coupled analysis approach to the low power transformer, it is possible to observe the

temperature rise due to the losses generation and the increase of the resistive loss due to the temperature rise in the windings. Besides that, the losses obtained by the electromagnetic model corresponds to a non-uniform heat generation accordingly to the magnetic flux density in the core and current density distribution in the windings This coupled methodology was developed to assist in the design process and optimization of electric machines, and also in the derating process for conditions different from the rated ones, for instance, higher ambient temperature, different levels of altitude and other factors that may affect the device performance and lifetime. Therefore, with this analysis methodology, it is possible to obtain a wider view of the machine performance without the time and financial resources of building various prototypes.

By using a study case of a simple electric machine, it was possible to understand the methods' main advantages and disadvantages. Moreover, from the results obtained the models presented satisfactory results when compared to the experimental data.

This work dealt with the thermal model of electric machines that has been receiving more attention in the past years, also presented a coupled analysis methodology, that is a trending method due to the advances in the computer-aided engineer software.

6.1 Future Work

The first issues to improve is the experimental thermal data of the transformer. As discussed in chapter 5**,** the thermal images do not give useful information about the transformer's core temperature and only provides the surfaces' temperature. Therefore, the objective is to use of thermal sensors, for instance, PT100, to measure the temperature of relevant spots, e.g., between windings and, between windings and core. Also, there is room for improvement in the thermal models, especially in the TRN model, which presented significant error when compared to the experimental temperature of the windings. The use of experimental thermal coefficients rather than empirical ones should increase the accuracy of the model, besides a more refined calculation of the convection on the TRN model

As the electromagnetic and thermal coupling model simulates a more realistic operation of the device, the use of the coupled model to build a digital twin would enable to exploit other important aspects of the device beyond the design process. A digital twin can be defined as computer-based models that are simulating, emulating, mirroring the

life of a physical entity, a digital twin is the virtual counterpart of a physical object [78]. That in the context of this work would be the electric machine modelled. Helping in the monitoring of the device in its application, enabling to keep track on the ageing factor of the materials, such as the insulation materials, also allowing to manage the predictive maintenance better and predict faults [79]–[81], which can be crucial for applications where the maintenance programs are of difficult implementation [82], [83].

Furthermore, future work should apply the electromagnetic and thermal coupled analysis to other electric machines, e.g., permanent magnet synchronous machines, induction motors, high power transformers. In addition, a more significant study on the iron loss modelling should consider its temperature dependency.

Bibliography

[1] IEA, “World electricity final consumption by sector, 1974-2018,” 2020. https://www.iea.org/data-and-statistics/charts/world-electricity-final-consumption-by-sector-1974-2018 (accessed Oct. 27, 2020).

[2] R. Marius *et al.*, *Multiphysics Simulation by Design for Electrical Machines, Power Electronics, and Drives*. John Wiley & Sons, 2018.

[3] E. Schmidt, “Finite element analysis of electrical machines and transformers: State of the art and future trends,” *COMPEL - Int. J. Comput. Math. Electr. Electron. Eng.*, vol. 30, no. 6, pp. 1899–1913, 2011, doi: 10.1108/03321641111168183.

[4] J. Pyrhönen, T. Jokinen, and V. Hrabovcová, *Design of Rotating Electrical Machines*. John Wiley & Sons, 2008.

[5] D. Staton, A. Boglietti, and A. Cavagnino, “Solving the more difficult aspects of electric motor thermal analysis,” *IEMDC 2003 - IEEE Int. Electr. Mach. Drives Conf.*, vol. 2, no. 3, pp. 747–755, 2003, doi: 10.1109/IEMDC.2003.1210320.

[6] M. Popescu *et al.*, “Modern Heat Extraction Systems for Electrical Machines – A Review,” pp. 289–296, 2015.

[7] G. Du, W. Xu, N. Huang, X. Cheng, and X. Xiao, “Rotor Design of High Power High Speed Permanent Magnet Machine Considering Multiphysics Constraints,” *2019 22nd Int. Conf. Electr. Mach. Syst. ICEMS 2019*, vol. 1, 2019, doi: 10.1109/ICEMS.2019.8921870.

[8] Z. Huang and J. Fang, “Multiphysics Design and Optimization of High-Speed Permanent-Magnet Electrical Machines for Air Blower Applications,” *IEEE Trans. Ind. Electron.*, vol. 63, no. 5, pp. 2766–2774, 2016, doi: 10.1109/TIE.2016.2518121.

[9] Y. Yasa, M. Elamin, Y. Sozer, J. Kutz, J. S. Tylenda, and R. L. Wright, “Acoustic noise mitigation for high pole count switched reluctance machines through skewing method with multiphysics FEA simulations,” *2017 IEEE Energy Convers. Congr. Expo. ECCE 2017*, vol. 2017-Janua, no. 1, pp. 738–744, 2017, doi: 10.1109/ECCE.2017.8095858.

[10] C. Yan, Y. Wei, C. Xu, and B. Zhang, “Experimental verification and electromagnetic-mechanics-acoustic field coupling analysis of transformer pressure relief valve malfunctions due to external short-circuit faults,” *IEEE Trans. Magn.*, vol. 55, no. 6,

pp. 9–12, 2019, doi: 10.1109/TMAG.2019.2900660.

[11] T. Ohinata and K. Arimatsu, “Reluctance Network Model of Three-Phase-Laminated-Core,” *IEEE Trans. Magn.*, vol. 55, no. 7, pp. 1–6, 2019, doi: 10.1109/TMAG.2019.2900527.

[12] E. M. Barhoumi, F. Wurtz, C. Chillet, and B. Ben Salah, “Reluctance network model for linear switched reluctance motor,” *12th Int. Multi-Conference Syst. Signals Devices, SSD 2015*, pp. 1–4, 2015, doi: 10.1109/SSD.2015.7348156.

[13] A. A. Diriye, Y. Amara, and G. Barakat, “Three-Dimensional Modeling of Permanents Magnets Synchronous Machines Using a 3D Reluctance Network,” *Proc. - 2018 23rd Int. Conf. Electr. Mach. ICEM 2018*, pp. 2304–2310, 2018, doi: 10.1109/ICELMACH.2018.8506820.

[14] C. Freitag, “Magnetic Properties of Electrical Steel, Power Transformer Core Losses and Core Design Concepts,” Elektrotechnik und Informationstechnik des Karlsruher Institutes für Technologie (KIT), 2017.

[15] L. Susnjic, Z. Haznadar, and Z. Valkovic, “3D finite-element determination of stray losses in power transformer,” *Electr. Power Syst. Res. J.*, vol. 78, pp. 1841–1818, 2008.

[16] S. Xue, J. Feng, S. Guo, J. Peng, W. Q. Chu, and Z. Q. Zhu, “A new iron loss model for temperature dependencies of hysteresis and eddy current losses in electrical machines,” *IEEE Trans. Magn.*, vol. 54, no. 1, 2018, doi: 10.1109/TMAG.2017.2755593.

[17] D. Lin, P. Zhou, W. N. Fu, Z. Badics, and Z. J. Cendes, “A Dynamic Core Loss Model for Soft Ferromagnetic and Power Ferrite Materials in Transient Finite Element Analysis,” *1318 IEEE Trans. Magn.*, vol. 40, no. 2, pp. 1318–1321, 2004.

[18] A. Boglietti, A. Cavagnino, D. Staton, M. Shanel, M. Mueller, and C. Mejuto, “Evolution and modern approaches for thermal analysis of electrical machines,” *IEEE Trans. Ind. Electron.*, vol. 56, no. 3, pp. 871–882, 2009, doi: 10.1109/TIE.2008.2011622.

[19] T. A. Jankowski *et al.*, “Development and validation of a thermal model for electric induction motors,” *IEEE Trans. Ind. Electron.*, vol. 57, no. 12, pp. 4043–4054, 2010, doi: 10.1109/TIE.2010.2043044.

[20] A. Boglietti, A. Cavagnino, M. Lazzari, and M. Pastorelli, “A Simplified Thermal Model for Variable-Speed Self-Cooled Industrial Induction Motor,” *IEEE Trans. Ind.*

Appl., vol. 39, no. 4, pp. 945–952, 2003, doi: 10.1109/TIA.2003.814555.

[21] M. Cavazzuti, G. Gaspari, S. Pasquale, and E. Stalio, "Thermal management of a Formula E electric motor: Analysis and optimization," *Appl. Therm. Eng.*, vol. 157, no. May, p. 113733, 2019, doi: 10.1016/j.applthermaleng.2019.113733.

[22] S. Nategh, H. Zhang, O. Wallmark, A. Boglietti, T. Nassen, and M. Bazant, "Transient Thermal Modeling and Analysis of Railway Traction Motors," *IEEE Trans. Ind. Electron.*, vol. 66, no. 1, pp. 79–89, 2019, doi: 10.1109/TIE.2018.2821619.

[23] Y. Xie and Y. Wang, "3D temperature field analysis of the induction motors with broken bar fault," *Appl. Therm. Eng.*, vol. 66, no. 1–2, pp. 25–34, 2014, doi: 10.1016/j.applthermaleng.2014.02.008.

[24] M. Allahbakhshi and M. Akbari, "Heat analysis of the power transformer bushings using the finite element method," *Appl. Therm. Eng.*, vol. 100, pp. 714–720, 2016, doi: 10.1016/j.applthermaleng.2016.02.065.

[25] D. Sarkar and A. K. Naskar, "Computation of thermal condition in an induction motor during reactor starting," *Int. J. Electr. Power Energy Syst.*, vol. 44, no. 1, pp. 938–948, 2013, doi: 10.1016/j.ijepes.2012.08.004.

[26] E. Galloni, P. Parisi, F. Marignetti, and G. Volpe, "CFD analyses of a radial fan for electric motor cooling," *Therm. Sci. Eng. Prog.*, vol. 8, no. September, pp. 470–476, 2018, doi: 10.1016/j.tsep.2018.10.003.

[27] M. Satrústegui, G. Artetxe, I. Elosegui, M. Martinez-Iturralde, and J. C. Ramos, "Wafter design for totally enclosed electric machines," *Appl. Therm. Eng.*, vol. 129, pp. 93–105, 2018, doi: 10.1016/j.applthermaleng.2017.10.011.

[28] J. Pyrhönen, P. Lindh, M. Polikarpova, E. Kurvinen, and V. Naumanen, "Heat-transfer improvements in an axial-flux permanent-magnet synchronous machine," *Appl. Therm. Eng.*, vol. 76, pp. 245–251, 2015, doi: 10.1016/j.applthermaleng.2014.11.003.

[29] A. . Fitzgerald, *Electric Machinery, Sixth Edition*, 6th ed. McGraw-Hill, 2003.

[30] M. N. O. Sadiku, *Elements of Electromagnetics*, Sixth. Oxford University Press, 2015.

[31] C. D. Graham, "Physical origin of losses in conducting ferromagnetic materials," *J. Appl. Phys.*, vol. 53, no. August, 1982, doi: 10.1063/1.330306.

[32] S. N. Vukosavic, *Electrical Machines*, 1st ed. Springer, 2013.

[33] D. Eggers, S. Steentjes, and K. Hameyer, "Advanced iron-loss estimation for nonlinear material behavior," *IEEE Trans. Magn.*, vol. 48, no. 11, pp. 3021–3024,

2012, doi: 10.1109/TMAG.2012.2208944.

[34] W. Roshen, “Iron loss model for permanent-magnet synchronous motors,” *IEEE Trans. Magn.*, vol. 43, no. 8, pp. 3428–3434, 2007, doi: 10.1109/TMAG.2007.899687.

[35] Giorgio Bertotti, “General properties of power losses in soft ferromagnetic materials,” *IEEE Trans. Magn.*, vol. 24, no. 1, pp. 621–630, 1988.

[36] A. Boglietti, A. Cavagnino, M. Lazzari, and M. Pastorelli, “Predicting iron losses in soft magnetic materials with arbitrary voltage supply: An engineering approach,” *IEEE Trans. Magn.*, vol. 39, no. 2 II, pp. 981–989, 2003, doi: 10.1109/TMAG.2003.808599.

[37] W. A. Roshen, “A practical, accurate and very general core loss model for nonsinusoidal waveforms,” *IEEE Trans. Power Electron.*, vol. 22, no. 1, pp. 30–40, 2007, doi: 10.1109/TPEL.2006.886608.

[38] J. Reinert, A. Brockmeyer, and R. W. A. A. De Doncker, “Calculation of losses in ferro- and ferrimagnetic materials based on the modified Steinmetz equation,” *IEEE Trans. Ind. Appl.*, vol. 37, no. 4, pp. 1055–1061, 2001, doi: 10.1109/28.936396.

[39] M. Albach, T. Duerbaum, and A. Brockmeyer, “Calculating core losses in transformers for arbitrary magnetizing currents a comparison of different approaches,” *PESC Rec. - IEEE Annu. Power Electron. Spec. Conf.*, vol. 2, pp. 1463–1468, 1996, doi: 10.1109/pesc.1996.548774.

[40] D. C. Hanselman, *Brushless Permanent Magnet Motor Design*, 2nd ed., vol. 26, no. 3. The Writer’s Collective, 2006.

[41] K. Yamazaki and Y. Kato, “Iron loss analysis of interior permanent magnet synchronous motors by considering mechanical stress and deformation of stators and rotors,” *IEEE Trans. Magn.*, vol. 50, no. 2, pp. 22–25, 2014, doi: 10.1109/TMAG.2013.2282187.

[42] M. Nakano *et al.*, “High-Precision calculation of iron loss by considering stress distribution of magnetic core,” *IEEJ Trans. Ind. Appl.*, vol. 129, no. 11, pp. 1060–1067, 2009, doi: 10.1541/ieejias.129.1060.

[43] M. Satoh, S. Kaneko, M. Tomita, S. Doki, and S. Okuma, “Stator shape improvement to decrease iron loss caused by shrink fit utilizing physical properties of electrical steel sheet,” *IEEJ Trans. Ind. Appl.*, vol. 127, no. 1, pp. 60–68, 2007, doi:

10.1541/ieejias.127.60.

[44] J. Chen, D. Wang, Y. Jiang, X. Teng, S. Cheng, and J. Hu, "Examination of Temperature-Dependent Iron Loss Models Using a Stator Core," *IEEE Trans. Magn.*, vol. 54, no. 11, 2018, doi: 10.1109/TMAG.2018.2829632.

[45] J. Driesen, R. Belmans, and K. Hameyer, "Methodologies for coupled transient electromagnetic-thermal finite element modeling of electrical energy transducers," *IEMDC 2001 - IEEE Int. Electr. Mach. Drives Conf.*, pp. 681–686, 2001, doi: 10.1109/IEMDC.2001.939387.

[46] F. P. Incropera, D. P. Dewitt, T. L. Bergman, and A. S. Lavine, *Fundamentals of Heat and Mass Transfer*, 6th ed. John Wiley & Sons, 2006.

[47] Y. A. Cengel, *Heat Transfer A Practical Approach*, 2nd ed. Mcgraw-Hill, 2002.

[48] M. Popescu, D. A. Staton, A. Boglietti, A. Cavagnino, D. Hawkins, and J. Goss, "Modern Heat Extraction Systems for Power Traction Machines - A Review," *IEEE Trans. Ind. Appl.*, vol. 52, no. 3, pp. 2167–2175, 2016, doi: 10.1109/TIA.2016.2518132.

[49] M. Li, Y. An, and Z. Zhang, "Improving Thermal Analysis Accuracy of LPTN for Vehicle Claw-Pole Alternator by Calibrating Forced Convection Coefficients Based on Experimental Results," *IEEE Access*, vol. 7, pp. 129327–129334, 2019, doi: 10.1109/ACCESS.2019.2940508.

[50] R. Shafaie, M. Kalantar, and A. Gholami, "Thermal Analysis of 10-MW-Class Wind Turbine HTS Synchronous Generator," vol. 24, no. 2, 2014.

[51] M. Jaritz and J. Biela, "Analytical model for the thermal resistance of windings consisting of solid or litz wire," *2013 15th Eur. Conf. Power Electron. Appl.*, pp. 1–10, 2013, doi: 10.1109/EPE.2013.6634624.

[52] R. Wrobel, S. Ayat, and J. L.Baker, "Analytical Methods for Estimating Equivalent Thermal Conductivity in Impregnated Electrical Windings.pdf," *2017 IEEE Int. Electr. Mach. Drives Conf.*, pp. 1–8, 2017, doi: 10.1109/IEMDC.2017.8002003.

[53] H. Liu, S. Ayat, R. Wrobel, and C. Zhang, "Comparative study of thermal properties of electrical windings impregnated with alternative varnish materials," *J. Eng.*, vol. 2019, no. 17, pp. 3736–3741, 2019, doi: 10.1049/joe.2018.8198.

[54] A. Boglietti *et al.*, "Equivalent Thermal Conductivity Determination of Winding Insulation System by Fast Experimental Approach," *2015 IEEE Int. Electr. Mach. Drives Conf.*, pp. 1215–1220, 2015, doi: 10.1109/IEMDC.2015.7409216.

[55] S. Ayat, R. Wrobel, J. Goss, and D. Drury, "Equivalent Thermal Conductivity for Impregnated Electrical Windings Formed from Profiled Rectangular Conductors . In 8th IET International Conference on Power Electronics , Machines and Drives (PEMD 2016) Estimation of Equivalent Thermal Conductivity fo," *8th IET Int. Conf. Power Electron. Mach. Drives (PEMD 2016)*, pp. 1–6, 2016, doi: 10.1049/cp.2016.0313.

[56] J. . Holman, *Heat Transfer*, 10th ed. Mcgraw-Hill, 2010.

[57] A. Boglietti, A. Cavagnino, M. Parvis, S. Member, and A. Vallan, "Evaluation of Radiation Thermal Resistances in Industrial Motors," *IEEE Trans. Ind. Appl.*, vol. 42, no. 3, pp. 688–693, 2006, doi: 10.1109/TIA.2006.873655.

[58] NI, "Multisim." 2015.

[59] P. Dechaumphai and S. Sucharitpwatskul, *Finite Element Analysis with ANSYS Workbench*. Alpha Science International LTD, 2018.

[60] M. N. O. Sadiku, *Numerical Techniques in Electromagnetics*, 2nd ed. CRC Press, 2000.

[61] İ. H. Teke, Y. Özüpak, M. S. Mamiş, E. E. B. Thermal, and P. Plant, "Electromagnetic Field and Total Loss Analysis of Transformers by Finite Element Method Abstract :," vol. 8, no. 1, pp. 24451–24460, 2019, doi: 10.18535/ijecs/v8i1.01.

[62] M. Yazdani-Asrami, M. Mirzaie, and A. A. Shayegani Akmal, "No-load loss calculation of distribution transformers supplied by nonsinusoidal voltage using three-dimensional finite element analysis," *Energy*, vol. 50, no. 1, pp. 205–219, 2013, doi: 10.1016/j.energy.2012.09.050.

[63] D. M. Ionel, M. Popescu, S. J. Dellinger, T. J. E. Miller, R. J. Heideman, and M. I. McGilp, "On the variation with flux and frequency of the core loss coefficients in electrical machines," *IEEE Trans. Ind. Appl.*, vol. 42, no. 3, pp. 658–667, 2006, doi: 10.1109/TIA.2006.872941.

[64] S. Kül, O. Bilgin, and M. Mutluer, "Application of Finite Element Method to Determine the Performances of the Line Start Permanent Magnet Synchronous Motor," *Procedia - Soc. Behav. Sci.*, vol. 195, pp. 2586–2591, 2015, doi: 10.1016/j.sbspro.2015.06.458.

[65] L. Hu, K. Yang, C. Suo, Y. Ding, and W. Yu, "Analysis of Radial Electromagnetic Force in Permanent Magnet Machine with Manufacturing Tolerance," *ICEMS 2018 - 2018 21st Int. Conf. Electr. Mach. Syst.*, pp. 256–260, 2018, doi:

10.23919/ICEMS.2018.8549530.

[66] H. H. Hanafy, T. M. Abdo, and A. A. Adly, "2D finite element analysis and force calculations for induction motors with broken bars," *Ain Shams Eng. J.*, vol. 5, no. 2, pp. 421–431, 2014, doi: 10.1016/j.asej.2013.11.003.

[67] Ansys, "Ansys® Academic Research Maxwell, Release 2019 R3." 2019.

[68] UGINE ACIERS DE CHATILLON ET GUEUGNON, "Fe V 470 - 50 HA." 2011.

[69] ANSYS, "Maxwell Help," 2019. www.ansys.com (accessed Mar. 26, 2020).

[70] T. Matsushita, *Electricity and magnetism : new formulation by introduction of superconductivity*. 2014.

[71] R. Sitar, I. Šulc, and Ž. Janić, "Prediction of local temperature rise in power transformer tank by FEM," *Procedia Eng.*, vol. 202, pp. 231–239, 2017, doi: 10.1016/j.proeng.2017.09.710.

[72] Ansys, "Ansys® Academic Research Mechanical, Release 2019 R3." 2019.

[73] S. Balci, I. Sefa, and N. Altin, "Design and analysis of a 35 kVA medium frequency power transformer with the nanocrystalline core material," *Int. J. Hydrogen Energy*, vol. 42, no. 28, pp. 17895–17909, 2017, doi: 10.1016/j.ijhydene.2017.03.158.

[74] D. Arumugam, P. Logamani, and S. Karuppiah, "Electromagnetic & thermal analysis of synchronous generator with different rotor structures for aircraft application," *Alexandria Eng. J.*, vol. 57, no. 3, pp. 1447–1457, 2018, doi: 10.1016/j.aej.2017.03.020.

[75] I. ANSYS, "Ansys® Academic Research Workbench, Release 2019 R3." 2019.

[76] G. LWW, "Technical data for Winding Wire." http://www.lww.se/wp-content/uploads/2017/06/LWW-brochure-2016.pdf (accessed Feb. 10, 2020).

[77] IEC, *IEC 60034-1 Rotating Electrical Machines - Rating and Performance*. IEC, 2017.

[78] B. R. Barricelli, E. Casiraghi, and D. Fogli, "A survey on digital twin: Definitions, characteristics, applications, and design implications," *IEEE Access*, vol. 7, no. Ml, pp. 167653–167671, 2019, doi: 10.1109/ACCESS.2019.2953499.

[79] J. Wang, L. Ye, R. X. Gao, C. Li, and L. Zhang, "Digital Twin for rotating machinery fault diagnosis in smart manufacturing," *Int. J. Prod. Res.*, vol. 57, no. 12, pp. 3920–3934, 2019, doi: 10.1080/00207543.2018.1552032.

[80] P. Aivaliotis, K. Georgoulias, and G. Chryssolouris, "The use of Digital Twin for predictive maintenance in manufacturing," *Int. J. Comput. Integr. Manuf.*, vol. 32,

no. 11, pp. 1067–1080, 2019, doi: 10.1080/0951192X.2019.1686173.

[81] Y. Yang *et al.*, “State Evaluation of Power Transformer Based on Digital Twin,” *Proc. - IEEE Int. Conf. Serv. Oper. Logist. Informatics 2019, SOLI 2019*, pp. 230–235, 2019, doi: 10.1109/SOLI48380.2019.8955043.

[82] K. Sivalingam, M. Sepulveda, M. Spring, and P. Davies, “A Review and Methodology Development for Remaining Useful Life Prediction of Offshore Fixed and Floating Wind turbine Power Converter with Digital Twin Technology Perspective,” *Proc. - 2018 2nd Int. Conf. Green Energy Appl. ICGEA 2018*, pp. 197–204, 2018, doi: 10.1109/ICGEA.2018.8356292.

[83] S. S. Johansen, “On Developing a Digital Twin for Fault Detection in Drivetrains of Offshore Wind Turbines,” no. June, 2018.

Appendix A

Transformer Characterization

A. Transformer Characterization

In this appendix the low poer shell-type single-phase transformer used during this work as study case will be detailed. This transformer was chosen as the object of study due to its simplicity, not having moving parts and its disponiblity on the laboratory. Figure A.1 shows the device used and its nameplate.

(a) (b)

Figure A.1 Single-phase transformer (a) and its nameplate (b).

Figure A.2 shows the configuration of the windings, that was determined by analysing the windings' wire diameter since the rated current of the low voltage winding is higher than the rated current of the high voltage winding, the wire with a larger diameter will correspond to the low voltage winding, which was present on the outer winding, thus the high voltage winding is inner winding. It was possible to measure only the diameter of the low voltage winding that is 2 mm. In the device's nameplate was identified the rated electric specifications, the rated power is 1 KW, and the rated voltage of 220 V for the primary winding and 110 V to the secondary winding, hence the rated transformation ratio is 2:1.

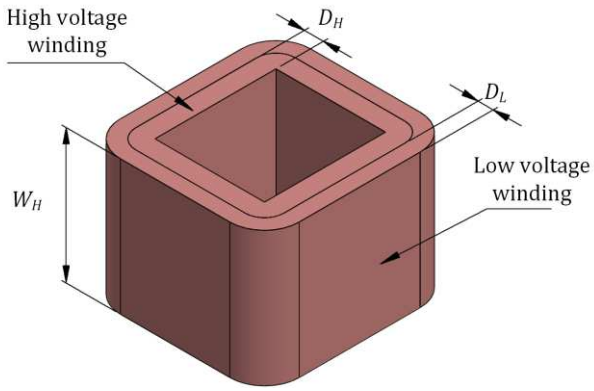

Figure A.2 Windings configuration.

To obtain the device's resistive and iron losses at room temperature (20 °C) a short-circuit and a no-load test were performed. Table A.1 summarizes the experimental data measured. The short-circuit test was accomplished by supplying the primary winding with its rated current and the short-circuiting the secondary winding, with this configuration the voltage applied in the primary winding is minimal, therefore the iron loss can be ignored and the power measured corresponds to the resistive loss at nominal load. In the no-load test, the primary winding was excited by its rated voltage (220 V) and the secondary winding was in open-circuit configuration, since the current flowing through the winding is small the resistive loss is minimal, therefore the power measured in this test corresponds to the transformer's iron loss. Also, in the no-load test, it is measured the real transformation ratio that is 220:116.

Table A.1 Transformer tests data at room temperature.

	V_1 (V)	I_1 (A)	V_2 (V)	I_2(A)	P (W)	R_1 (Ω)	R_2 (Ω)
Short-circuit	9.62	4.51	-	8.55	49.60	1.0	0.4
No-load	220	174×10^{-3}	116	-	13		

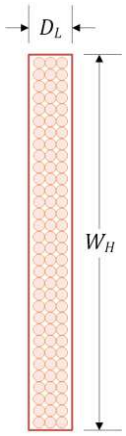

Figure A.3 Low voltage winding cross-section.

The number of turns of each winding was not specified by the manufacturer, therefore it is necessary to estimate it. It is known the wire's diameter of the low voltage winding, assuming that the number of turns fills the low voltage winding cross-sectional area, as shown in Figure A.3, the number of turns for the low voltage winding is given by,

$$N_2 \approx \frac{D_L W_H}{\pi r_2^2} \tag{A.1}$$

where r_2 is the wire radius of the winding, which results in $N_2 \approx 178$, and $N_1 \approx 338$ is obtained by using the real transformation ratio.

Figure A.4 shows the geometry parameters used to model the transformer along with the windings parameters (Figure A.2), and Table A.2 presents its respective values.

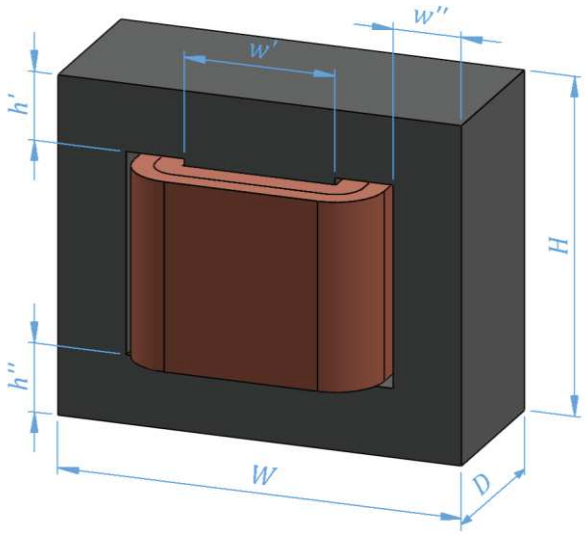

Figure A.4 Transformer core geometry parameters.

Table A.2 Transformer geometry parameters.

	Parameter	Dimension (mm)
Core	W	150.00
	w'	56.00
	w''	25.40
	H	125.33
	h'	25.07
	h''	25.40
	D	62.00
Windings	W_H	70.00
	D_L	8.00
	D_H	10.00

Appendix B

Thermal Parameters and Formulation

B. Thermal Parameters and Formulation

This appendix details the thermal properties of the materials used on the analytical and numerical thermal model of the transformer. Table B.1 summarizes the materials thermal and physical properties used in the models.

Table B.1 Materials thermal and physical properties. [4]

Material	Thermal conductivity k (W/°C/m)	Emissivity ε
Electrical steel sheet (lamination direction)	22-40	
Electrical steel sheet (direction normal to lamination)	0.6	
Treating varnish	0.26	
Black paint		0.9-0.95
Cast iron		0.3

The model used to calculate the thermal conductivity of the windings was shown in section 3.4.4, Table B.2 shows the parameters values used to obtain the thermal conductivity for each winding, the insulation thermal conductivity corresponds to a treating varnish typically used in electric machines [4].

Table B.2 Windings thermal conductivities parameters.

	k_i (W/m/°C)	d' (mm)	d (mm)	δ_i (mm)	k_{av} (W/m/°C)
High voltage winding	0.26	1.67	1.6	0.07	5.95
Low voltage winding		2.074	2	0.074	7.04

The convection coefficients were formulated by the relations found in [47] for free air convection, the relations used are presented in Table B.3.

Table B.3 Convection coefficients relations. (Adapted from [47]*.)*

Geometry	Convection coefficient (W/m²/°C)
Vertical plate or cylinder 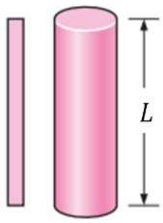	$h_{conv} = 1.42\left(\frac{\Delta T}{L}\right)^{0.25}$
Horizontal plate ($L = 4A/p$, being A the surface area and p the perimeter) 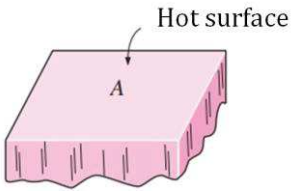 (a) Hot surface facing up	$h_{conv} = 1.32\left(\frac{\Delta T}{L}\right)^{0.25}$
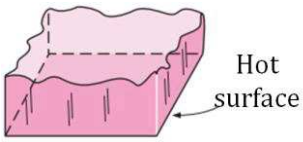 (b) Hot surface facing down	$h_{conv} = 0.59\left(\frac{\Delta T}{L}\right)^{0.25}$

By using the presented convection relations and the geometry parameters of the transformer presented in Figure A.4 and Figure A.2, the convection coefficients are formulated and shown in Table B.4.

Table B.4 Convection coefficients equations.

Convection coefficient (W/m²/°C)
$h_{c1} = 1.42\left(\frac{\Delta T}{h'}\right)^{0.25}$
$h_{c2} = 1.32\left[\frac{\Delta T}{\left(\frac{2DW}{D+W}\right)}\right]^{0.25}$
$h_{c3} = 1.42\left(\frac{\Delta T}{H}\right)^{0.25}$
$h_{w1} = 1.42\left(\frac{\Delta T}{W_H}\right)^{0.25}$
$h_{w2} = 1.32\left(\frac{\Delta T}{L}\right)^{0.25}$
$h_{w3} = 0.59\left(\frac{\Delta T}{L}\right)^{0.25}$
$L = 4\left[\frac{(w' + 2D_L + 2D_H)(D_L + D_H)}{2(w' + 2D_L + 2D_H) + 2(D_L + D_H)}\right]$

Transformer's Thermal Resistance Network Network

The TRN developed in section 3.4 was implemented on the circuit simulator Multisim. Figure B.1 shows the implemented TRN. Table B.5 shows the temperature results on the middle point of each element, and the temperature result for the surfaces in contact with the ambient. It is important to notice, that these results correspond to the TRN considering the transformer's losses at ambient temperature.

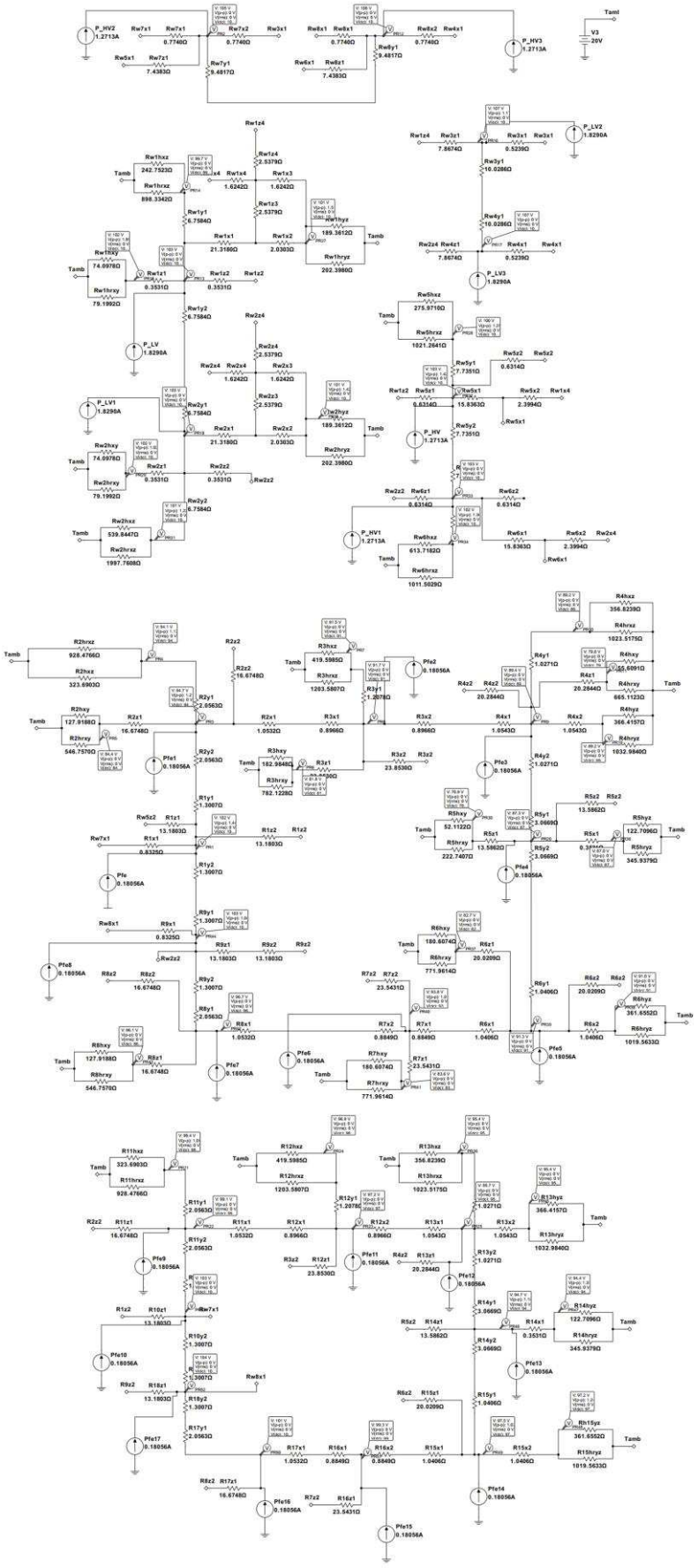

Figure B.1 Developed TRN considering the transformer's losses at ambient temperature

Table B.5 TRN temperature results considering the transformer's losses at ambient temperature

Volume Element	Middle Point Temperature (°C)	Surface *xy* Temperature (°C)	Surface *xz* Temperature (°C)	Surface *yz* Temperature (°C)
V_{w1}	103	102	99.7	101
V_{w2}	103	102	101	101
V_{w3}	107	-	-	-
V_{w4}	107	-	-	-
V_{w5}	103	-	100	-
V_{w6}	103	-	102	-
V_{w7}	105	-	-	-
V_{w8}	106	-	-	-
V_{c1}	102	-	-	-
V_{c2}	94.7	84.4	94.1	-
V_{c3}	91.7	81.8	91.5	-
V_{c4}	89.4	79.8	89.2	89.2
V_{c5}	87.3	70.9	-	87
V_{c6}	91.3	82.7	-	91
V_{c7}	93.8	83.6	-	-
V_{c8}	96.7	86.1	-	-
V_{c9}	103	-	-	-
V_{c10}	103	-	-	-
V_{c11}	99.1	-	98.4	-
V_{c12}	97.2	-	96.9	-
V_{c13}	96.7	-	95.4	95.4
V_{c14}	94.7	-	-	94.4
V_{c15}	97.5	-	-	97.2
V_{c16}	99.3	-	-	-
V_{c17}	101	-	-	-
V_{c18}	104	-	-	-

Figure B.2 shows the implemented TRN considering the transformer's losses at the steady-state temperature, and Table B.6 shows the temperature results on the middle point of each element, and the temperature result for the surfaces in contact with the ambient.

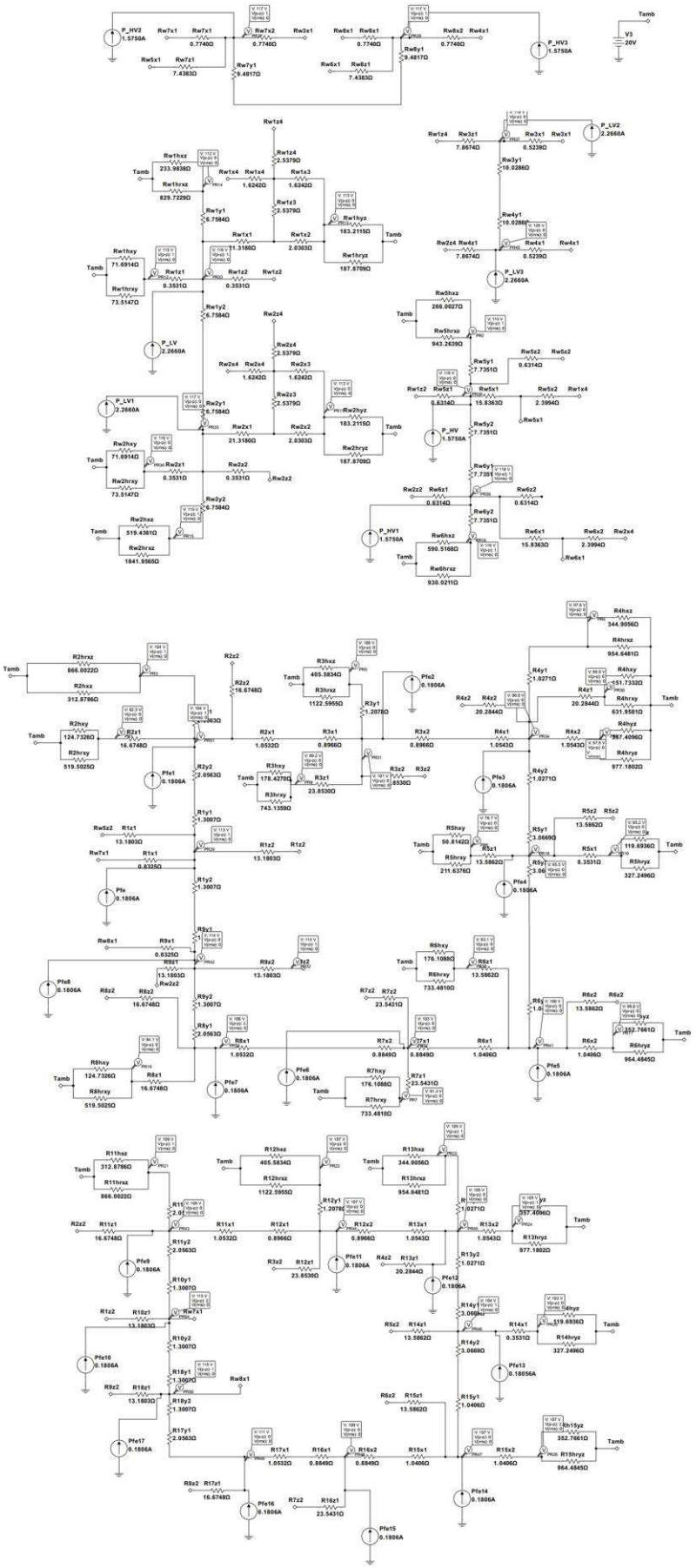

Figure B.2 Developed TRN considering the transformer's losses at the steady-state temperature

Table B.6 TRN temperature results considering the transformer's losses at the steady-state temperature

Volume Element	Middle Point Temperature (°C)	Surface *xy* Temperature (°C)	Surface *xz* Temperature (°C)	Surface *yz* Temperature (°C)
V_{w1}	116	115	112	113
V_{w2}	117	116	115	113
V_{w3}	119	-	-	-
V_{w4}	120	-	-	-
V_{w5}	116	-	113	-
V_{w6}	118	-	116	-
V_{w7}	117	-	-	-
V_{w8}	117	-	-	-
V_{c1}	113	-	-	-
V_{c2}	104	92.3	104	-
V_{c3}	101	89.2	100	-
V_{c4}	98	86.9	97.6	97.6
V_{c5}	95.5	76.7	-	95.2
V_{c6}	100	93.1	-	99.8
V_{c7}	103	91.3	-	-
V_{c8}	106	94.1	-	-
V_{c9}	114	-	-	-
V_{c10}	115	-	-	-
V_{c11}	109	-	109	-
V_{c12}	107	-	107	-
V_{c13}	105	-	105	105
V_{c14}	104	-	-	103
V_{c15}	107	-	-	109
V_{c16}	109	-	-	-
V_{c17}	111	-	-	-
V_{c18}	115	-	-	-